iScience

CellPress

Article

Random Walk Revisited: Quantification and Comparative Analysis of *Drosophila* Walking Trajectories

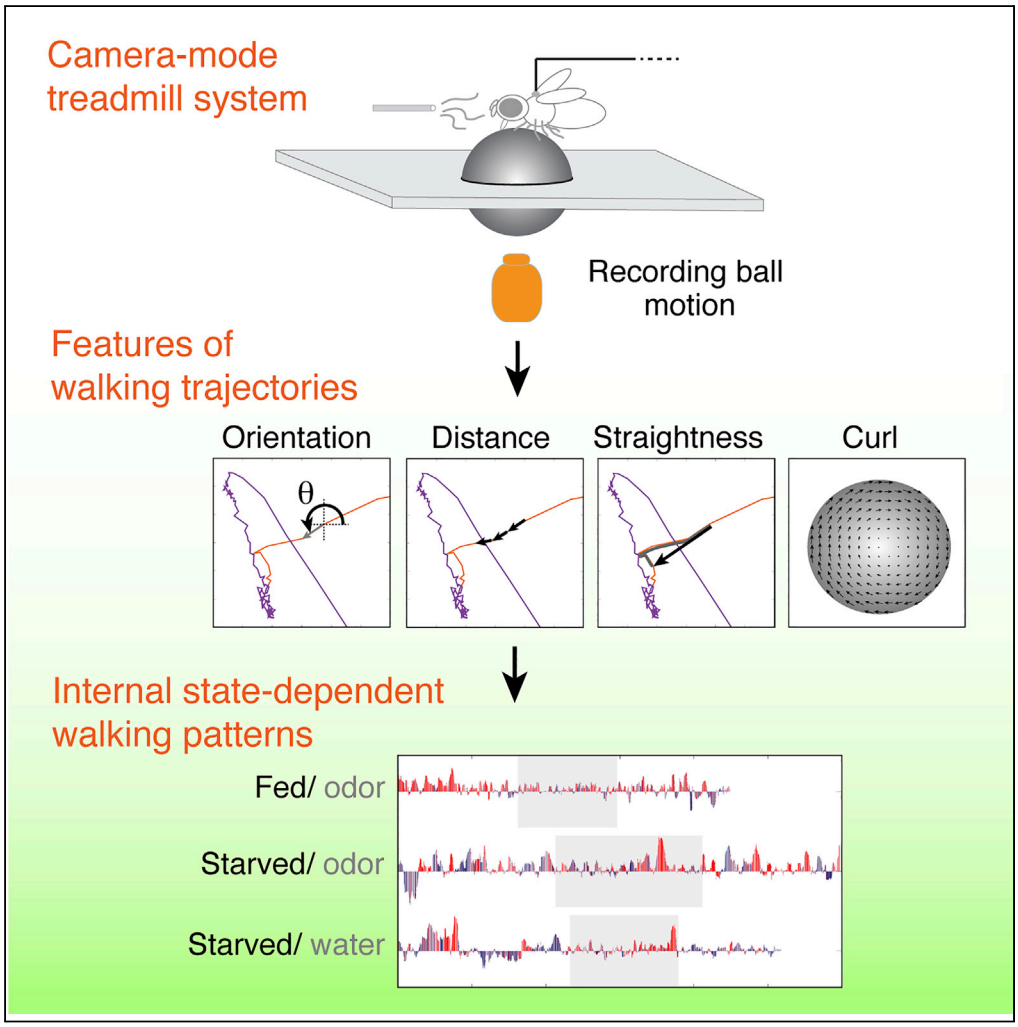

Kuo-Ting Tsai, Ya-Hui Chou

yhchou@gate.sinica.edu.tw

HIGHLIGHTS

A camera-mode treadmill system was built to track *Drosophila* walking trajectories

Four key features were identified to describe walking strategies

Ball rotation is indispensable for full characterization of trajectories

Fed and starved control flies show no obvious differences in their random walk

Tsai & Chou, iScience *19*, 1145–1159
September 27, 2019
https://doi.org/10.1016/j.isci.2019.08.054

iScience

CellPress

Article

Random Walk Revisited: Quantification and Comparative Analysis of *Drosophila* Walking Trajectories

Kuo-Ting Tsai[1] and Ya-Hui Chou[1,2,3,4,*]

SUMMARY

Walking trajectory is frequently measured to assess animal behavior. Air-supported spherical treadmills have been developed for real-time monitoring of animal walking trajectories. However, current systems for mice mainly employ computer mouse microcameras (chip-on-board sensors) to monitor ball motion, and these detectors exhibit technical issues with focus and rotation scale. In addition, computational methods to analyze and quantify the "random walk" of organisms are under-developed. In this work, we overcame the hurdle of frame-to-signal translation to develop a treadmill system with camera-based detection. Moreover, we generated a package of mathematical methods to quantify distinct aspects of *Drosophila* walking trajectories. By extracting and quantifying certain features of walking dynamics with high temporal resolution, we found that depending on their internal state, flies employ different walking strategies to approach environmental cues. This camera-based treadmill system and method package may also be applicable to monitor the walking trajectories of other diverse animal species.

INTRODUCTION

Animals continuously integrate dynamic multisensory cues while searching their ever-changing environment for food, mates, safety, or other objectives (Anderson and Perona, 2014; Dickinson et al., 2000; Greenspan and Ferveur, 2000). After compiling sensory information, neural circuits then translate it into movements with different trajectories, which can be observed and used as a readout for analysis. Animal trajectories can be either three-dimensional, such as those for flight and swimming, or two-dimensional, as for walking and crawling. As the movements of organisms are the products of multiple integrated neural circuits, the trajectories should exhibit signatures that distinguish them from models of non-biological movements, such as Brownian motion (Klafter et al., 1996; Dickinson et al., 2000). Lévy walk and Lévy flight are the best-established analyses to describe the "random walk/flight" of animal search strategies (Bartumeus et al., 2005; Rhee et al., 2011). In most experiments exploring animal motility, the random walk is used to describe the walking trajectories of control animals. However, starved animals are often used for olfactory and gustatory studies, and accumulating evidence suggests that internal state-dependent mechanisms are important determinants of walking trajectories (Van Breugel et al., 2018; Grunwald Kadow, 2019; Rengarajan et al., 2019). Whether control flies with distinct internal states exhibit similar random walk patterns remains unclear. Therefore, a better quantitative definition of random walk (at a millisecond timescale) is necessary. *Drosophila* is one of the most prevalent animal models for dissecting the connections between neural circuit integration and behavior (Gaudry et al., 2012b; Dickinson et al., 2000; Robie et al., 2017; Branson et al., 2009; Kabra et al., 2012; Dankert et al., 2009; Grover et al., 2016). Although many paradigms for assessing behavior have been established to evaluate animal movement under different physiological states and during different tasks (Kim and Dickinson, 2017; Semmelhack and Wang, 2009; Bahl et al., 2013; Coen et al., 2014; Gomez-Marin et al., 2011; Wu et al., 2014; Álvarez-Salvado et al., 2018; Bidaye et al., 2014; Reynolds and Frye, 2007), the quantitative analytical tools to analyze the measured trajectories remain under-developed.

Spherical treadmill systems have been developed to acquire walking trajectories or other behavioral features of different animals during the performance of tasks, such as navigation, osmotrophotaxis, olfactory discrimination, motion detection, auditory transduction, or gait control (Borst and Heisenberg, 1982; Takasaki et al., 2012; Radvansky and Dombeck, 2018; Kain et al., 2013; Buchner, 1976; Gaudry et al., 2012a; Kohatsu et al., 2011; Clark et al., 2011; Lehnert et al., 2013; Seelig et al., 2010; Bahl et al., 2015; Ribeiro et al., 2018). Notably, these systems have recently been adapted to incorporate visual or olfactory virtual reality,

[1]Institute of Cellular and Organismic Biology, Academia Sinica, Taipei 11529, Taiwan

[2]Neuroscience Program of Academia Sinica, Academia Sinica, Taipei 11529, Taiwan

[3]Genome and Systems Biology Degree Program, Academia Sinica and National Taiwan University, Taipei 10617, Taiwan

[4]Lead Contact

*Correspondence: yhchou@gate.sinica.edu.tw

https://doi.org/10.1016/j.isci.2019.08.054

creating a powerful tool for dissecting neural circuit activity and regulatory mechanisms (Seelig et al., 2010; Harvey et al., 2009; Radvansky and Dombeck, 2018; Sato et al., 2017; Haberkern et al., 2019; Kohatsu and Yamamoto, 2015; Runyan et al., 2017). Such treadmill systems require minimal delay time for closed-loop feedback and high precision of signals, both of which are largely determined by the detector that digitally records the motion of an air-supported ball. The most widely used treadmill systems for mice, rats, and flies utilize the sensor chips from a computer mouse to measure directional ball motion (Harvey et al., 2009; Seelig et al., 2010; Gaudry et al., 2012a; Kain et al., 2013; Radvansky and Dombeck, 2018; Haberkern et al., 2019; Kohatsu and Yamamoto, 2015). Such sensor chips offer high temporal resolution and directly report the displacements of ball surface. However, there are three major limitations with these sensor chip detectors. First, the distance between the sensor and the detected surface must be within the working distance of the sensor. If not, a compensatory optical design is necessary to acquire the motion of the ball. However, the fitting measurement for such compensatory optical design is lacking. Second, single optical computer mouse sensors are not able to monitor the rotation axis of the ball. Thus, if a sensor is pointed directly at the rotation axis, it will fail to report rotation of the ball. The use of two orthogonally aligned senor chips ensures the detection of ball rotation, but this design cannot give complete information about shifts in rotation axis. Third, validating the accuracy of signals from the computer mouse sensors remains challenging.

An alternative modality for animal treadmill detectors is to use a camera to track visible patterns on the ball surface (Moore et al., 2014). Such a "camera-mode" treadmill system would supply information about every pixel in a region of interest (ROI), but camera detectors also suffer from limitations. First, specular reflection on the ball surface may deteriorate the tracked patterns. This issue can be resolved by proper illumination of the ball surface. Second, the recorded contours of patterns on the ball surface will vary based on their positions. As such, patterns located in the central zone of the ROI will appear to be expanded, whereas the same patterns near the rim of the ball will be distorted. Third, an established model of ball patterns is required for reconstruction of ball motion from video frames (Moore et al., 2014). This limitation prevents camera-mode treadmill systems from being easily adapted by other laboratories.

In this study, we developed a new camera-mode treadmill system to bypass the issues of focus and lack of complete information about rotation that are common to "computer-mouse-mode" systems. Our system also overcomes a major limitation of camera-mode systems, as it does not require a pre-established model of visible markings on the ball (ball patterns). We successfully translated the captured frames into digital signals, and the calibration of odor arrival delay time with a photoionization detector (PID) allowed us to maximize temporal resolution at odor phase transitions. We identified four features of optically recorded ball motion to collectively describe individual walking patterns: rotation, distance, straightness, and curl. As a proof of principle, we used our system to measure the effects of internal state-dependent mechanisms on distinct walking strategies of single *Drosophila*. In addition, we revisited the idea of random walk in control flies, and interestingly, we did not observe differential walking patterns between starved and fed flies. Importantly, our camera-mode treadmill system is scalable, making it suitable for studies on other animal species in addition to *Drosophila*.

RESULTS

Camera-Mode Fly Treadmill System

To collect signals of ball motion that allow verifiable reconstruction of walking trajectories, we designed and built a camera-mode fly treadmill system (Figures 1A, 1B, and S1A, Video S1). In this system, the motion of an air-supported ball is driven by the walking maneuvers of a tethered fly. As the motion of an observed ball surface is symmetric to its opposite surface, we positioned the camera detector underneath the air-supported ball (Figure 1A). In previous float mounts of computer-mouse-mode treadmill systems, a single air outlet was sufficient to support the ball and allow a tethered fly to stand on top (Buchner, 1976; Seelig et al., 2010; Gaudry et al., 2012a; Kain et al., 2013; Haberkern et al., 2019; Kohatsu and Yamamoto, 2015; Clark et al., 2011; Bahl et al., 2015). However, a one-air-stream float mount may suffer from two potential drawbacks. First, air turbulence may occur during experimental sessions. Second, the walking fly may deliver enough force to the ball that is pushed into the margin of the air outlet. To overcome these issues, we designed a float mount with four air inlets (Figures 1A and S1B). The mutually counteracting airflow from four outlets largely eliminated the occasional air turbulence that occurs in float mounts with a single air outlet. This design also allowed us to position a high-speed charge-coupled device camera facing the bottom of the floating ball. A small 192 × 200-pixel area of the ball bottom was brought into focus, allowing frames to be acquired at 100 Hz (sampling time: 10 ms) (Figure 1C). We then developed a custom tracking

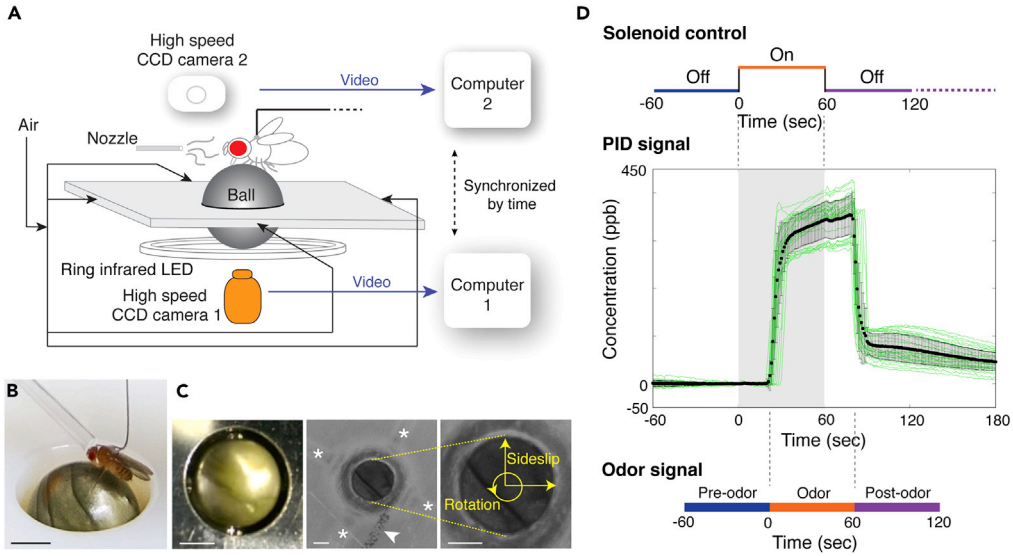

Figure 1. Fly Treadmill System

(A) The schematic diagram of the camera-mode fly treadmill system.

(B) Lateral view of a tethered fly walking on the ball suspended on the float mount.

(C) Bottom view of the ball (left panel). (Middle and right panels) A single frame of infrared video recording of ball motion. Asterisks mark the four air inlets. The arrowhead indicates a mark for positioning the nozzle.

(D) (Top) The on and off phases of the solenoid valves of the odor delivery system. (Middle) The dynamics of odor concentration (10^{-1} dilution of pentanoic acid) detected by photoionization detector (PID). Black dots indicate the average of 29 trials (green lines) and are shown as mean ± SD. Gray zone is the on phase of solenoid valves. Note a 22-s delay between the switching on of solenoid valves and the arrival of odor at a flow rate 17 mL/min. (Bottom) After calibration to the PID signal, the odor history can be divided as pre-odor (off, blue), during odor (on, orange), and post-odor (off, magenta) phases. All experimental data show odor delivery phases after PID signal correction, unless otherwise noted. Scale bars, 2 mm in (B) and 1 mm in (C).

See also Figures S1 and S2, and Video S1.

program in C++. The fundamental idea behind the tracking program is that for each frame, the pattern in the central zone of the air-supported ball is fitted with the previous frame. The displacement and the rotation of the pattern are then considered as motion in the X-Y plane and along the rotation axis. Note that in this work, "motion" and "movement" are used to specifically refer to the movements of the ball and the fly, respectively.

We also built an odor delivery system, consisting of a pipeline and nozzle, to flow-in odorants to the tethered fly (Figures 1D and S2). Delivery is controlled by four two-way solenoid valves (Figure 1D, top). To estimate the delay time between switching on odor flow with the solenoid valves and odor arrival at the fly, a PID was placed on the ball surface in the same position as a tethered fly (Figure S1E). In this system, the delay time was 22 s when the odor was delivered at 17 mL/min (middle panel in Figure 1D). Therefore the odor signal timing in our experiments was adjusted according to the measured delay time for the corresponding flow rate (bottom panel in Figure 1D).

Digitizing Fly Walking Trajectories

A major challenge in the development of our camera-mode treadmill system was digitizing fly walking trajectories from the video recording of ball motion. To this end, we tested four methods: gradients pyramid, grayscale value pyramid, low discrepancy sampling, and optic flow (Figure S3, Video S2). We found that the motion of tested object can be best translated from a serial set of frames using optic flow.

The ball motion videos were subjected to optic flow analysis to translate the frame information to flow vectors. The flow vectors were then used to generate five features: displacement along the x axis (X), displacement along the y axis (Y), rotation center at X, rotation center at Y, and curl (Figure 2A) (see Methods for a description of the relationships between rotation centers, yaw, roll, and pitch). X and Y were then further used to calculate

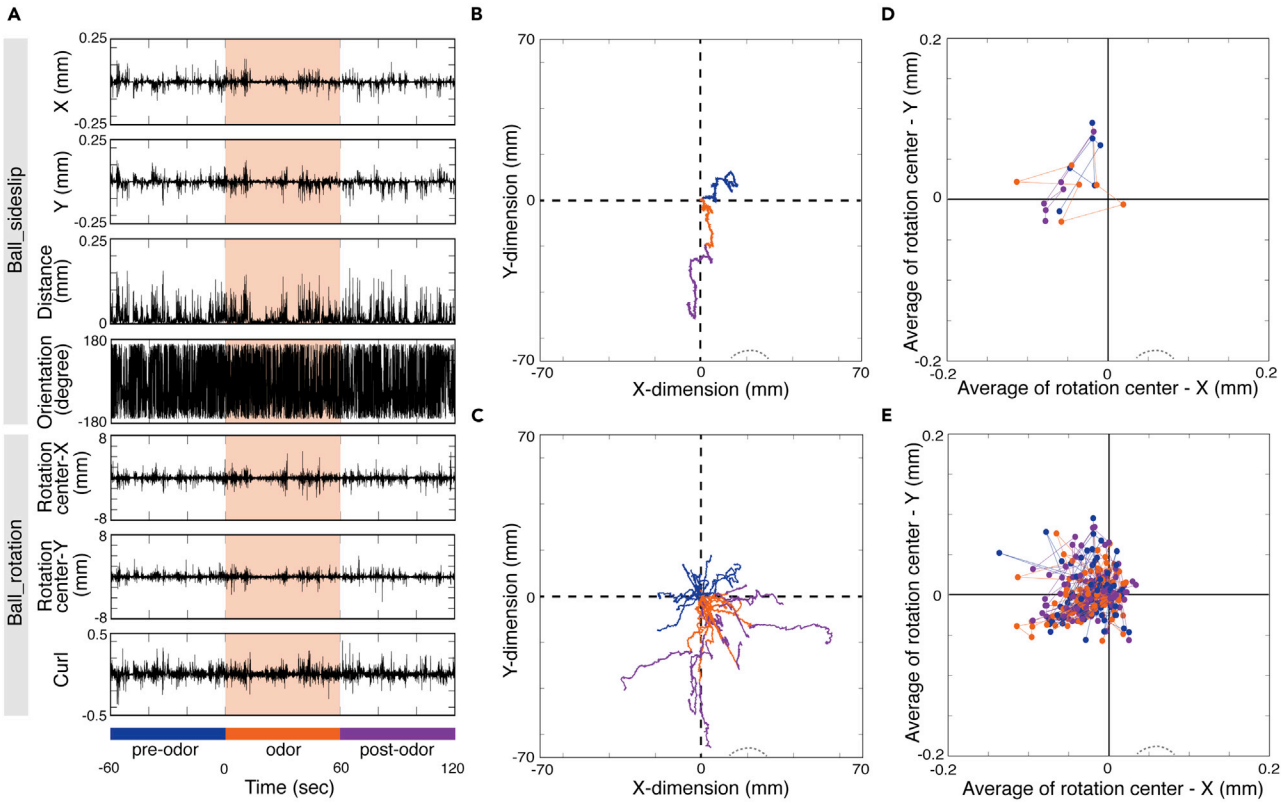

Figure 2. Reconstructing Fly Trajectories from Ball Motion

(A) (Top) Time history of starved fly-driven ball motion as displacement along X-dimension (X), displacement along Y-dimension (Y), distance, orientation, rotation center at X, rotation center at Y, and curl at every 10-ms interval (sampling time). The features were derived from the motion of the ball. The speed (mm/10 ms) has the same pattern as walking distance. Odor was a 10^{-1} dilution of pentanoic acid at 17 mL/min.

(B) A reconstructed walking trajectory of a starved fly according to the first two features in (A). Dashed-line contoured area indicates the direction of the nozzle. Color codes of odor phases are the same as (A).

(C) Reconstructed walking trajectories of 16 starved flies.

(D) The position of the ball rotation center derived from the same fly as in (B).

(E) The position of ball rotation centers derived from the same group of flies as in (C).

See also Figure S3 and Video S2.

the "distance" and "orientation," which stand for the magnitude and the direction of displacement in the X-Y plane, respectively (explained in detail below) (Figure 2A). Next, the first two features were integrated to reconstruct the walking trajectories of individual flies (Figures 2B and 2C). In addition, the ball rotation center can be reconstructed from rotation center-X and rotation center-Y (Figures 2D and 2E).

Flies with different internal states are expected to differentially value the same food odor or stimuli (Van Breugel et al., 2018; Grunwald Kadow, 2019). We therefore reasoned that flies with different internal states may show distinct walking patterns in response to the same environmental cues, and the trajectory features we measured should be sufficient to identify such differences. To test this hypothesis and validate our system, individual flies that were either fed or starved were placed on the ball of the treadmill system, and after some time, food odor or water vapor was administered. The seven distinct features of ball motion were extracted (Figures 3A–3C) and used to reconstruct the walking trajectories (Figures 3D–3F) and ball rotation centers (Figures 3G–3I) for single flies. As expected, we saw that flies with different internal states were likely to exhibit distinct walking trajectory patterns in response to environmental cues, odor, or water vapor (explained in detail below).

Flies in Different Internal Status Orientated the External Cues in Different Kinetics

Two ball motion features, displacement along the x axis and displacement along the y axis, were used to derive the orientation of a tested fly (Figure 4A). Orientation was calculated as the counterclockwise angle

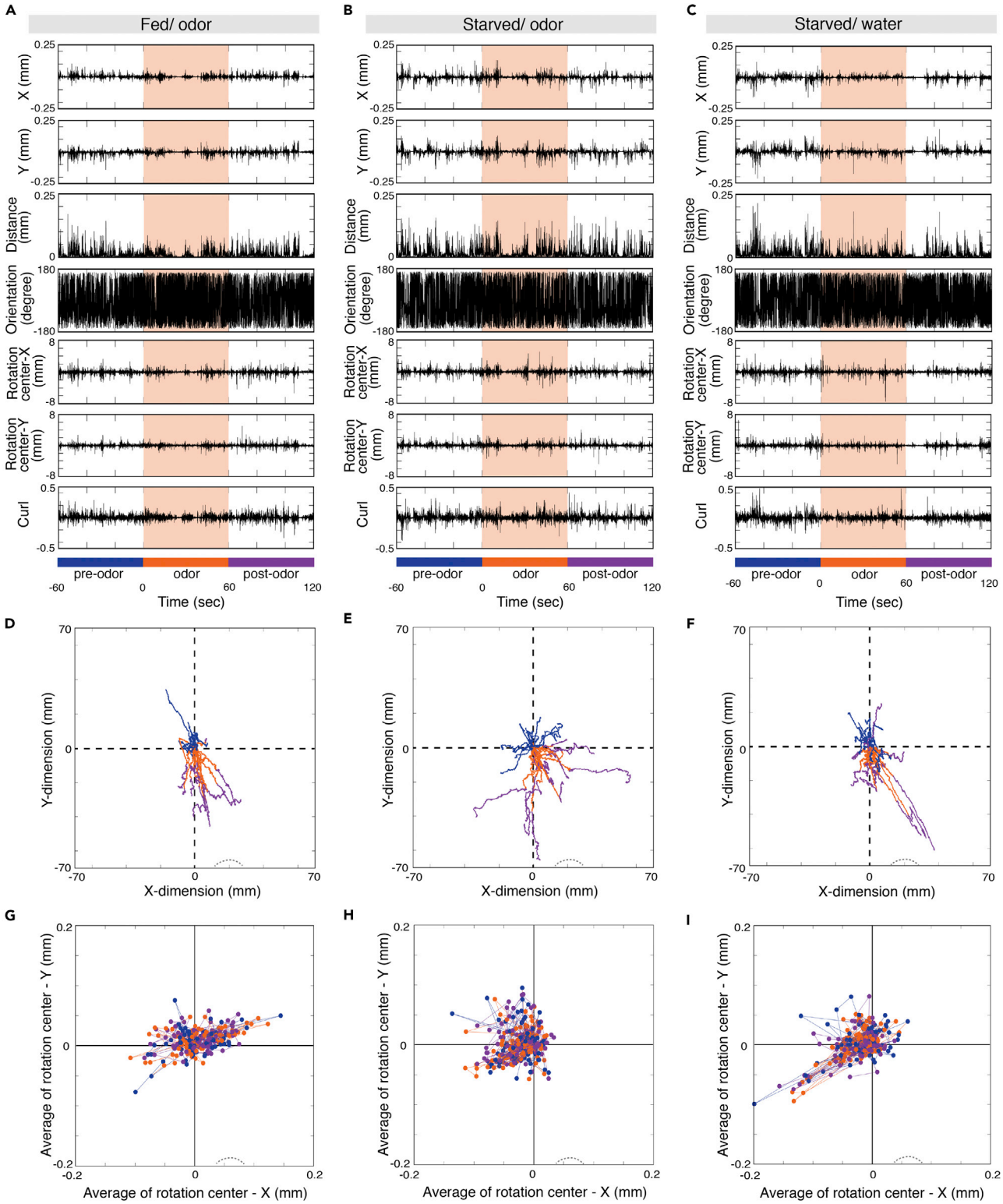

Figure 3. Trajectories Derived from Flies with Different Internal States Show Different Walking Characteristics

(A–C) Similar to Figure 2A, the panels show the time history of ball motion features driven by a fed fly in response to food odor (A), by a starved fly in response to food odor (B), and by a starved fly in response to water vapor (C). A 10^{-1} dilution of pentanoic acid or water vapor was applied at 17 mL/min. (B) The same data as shown in Figure 2A.

Figure 3. *Continued*

(D–F) Similar to Figure 2C, the panels show the reconstructed walking trajectories of 15 fed flies in response to food odor (D), 16 starved flies in response to food odor (E), and 17 starved flies in response to water vapor (F). (E) Same data as shown in Figure 2C.

(G–I) Similar to Figure 2E, the panels show the reconstructed rotation centers of 15 fed flies in response to food odor (G), 16 starved flies in response to food odor (H), and 17 starved flies in response to water vapor (I). (H) The same data as shown in Figure 2E.

(θ) between two sampling time points (middle panel in Figure 4A). Accordingly, the orientation dynamics of a representative fly in pre-odor, odor, and post-odor phases were reconstructed to an orientation distribution map (right panel in Figure 4A). In the example shown, the fly tended to orient itself to ~288° during odor and post-odor phases, which corresponds to the approximate position of nozzle (odor source covers the area from ~270° to 306°). Maps from all single flies in the same test group were then compiled and are shown as a normalized distribution map (Figure 4B). To better understand the individual variability of walking dynamics, we did not exclude statistical outliers; instead, all collected trajectories were used in the analyses.

Several factors, such as the genetic background of flies, the concentration of odor, and the speed of odor plume, may influence the results. To optimize the test conditions, we first examined the odor distribution maps of flies from five different genetic backgrounds (Figure S4A). We found that DL wild-type flies have most consistent orientation responses to odor, so we used DL wild-type flies in subsequent experiments.

The airflow delivery system for odor or water vapor has two potential effects on fly behavioral responses (Zhou and Wilson, 2012). First, the airflow itself produces shearing forces on flies. Second, the magnitude of airflow determines the dynamics of odor concentration and the delay time for the odor plume to reach the fly. Therefore, we examined the effects of odor delivery at 10, 17, and 22 mL/min on the orientation distributions of flies (Figure S4B). Flies from three experimental groups showed the most differential dynamic responses to odor delivered at 17 mL/min. Therefore, we used an odor delivery flow rate of 17 mL/min for subsequent experiments.

To address whether the internal state of a fly would affect its response toward a stimulus, we administered pentanoic acid food odor to either fed or starved DL flies. We found that both groups of flies effectively oriented themselves toward the odor, suggesting they were attracted by the food odor (comparing pre-odor and odor phases, Figure 4B). However, fed and starved flies showed different orientation dynamics across pre-odor, odor, and post-odor phases (Figures 4C and 4D). Starved flies tended to orient themselves toward the odor faster at the initial stage of odor phase; in contrast, fed flies tended to stay oriented toward the odor at late stage of odor phase. A similar response at the initial stage of the odor phase was also observed when water vapor was applied to starved flies (right panel, Figures 4B–4D). Such differences are unlikely to be the result of reduced locomotor activity in starved flies based on control experiments (Figure S5, Methods). These results suggested that starved flies respond more quickly to an environmental cue, no matter whether it is food odor or water. In addition, the same food odor may have different valence to starved and fed flies.

Flies with Different Internal States Exhibit Different Walking Patterns in Response to Environmental Cues

The first feature we extracted from the ball motion, orientation, was sufficient to show that flies with different internal states have distinct response dynamics to the same food odor. We next asked whether flies with different internal states tend to use different walking strategies to explore the environmental cues. In addition, we were interested to know whether flies with similar internal states exhibit different walking patterns in response to different external cues. To delineate these responses, we evaluated three additional features: distance, straightness (derived from displacement and distance), and curl (Figure 5). The dynamic changes in distance suggested that flies tend to walk longer for certain time after encountering food odor, but not water (Figures 5A and 5B). This movement pattern was particularly obvious in starved flies encountering food odor.

Straightness is a feature that describes the twists and turns of curves (Figure 5C, Methods) and was calculated in 5-s bins. For a given straightness close to 1, the path traversed by the fly is close to a straight line. More dynamic (changes in) straightness along time represents a higher frequency of a fly's walking trajectory alternating between straight lines and tortuous paths. Immediately upon and during administration of

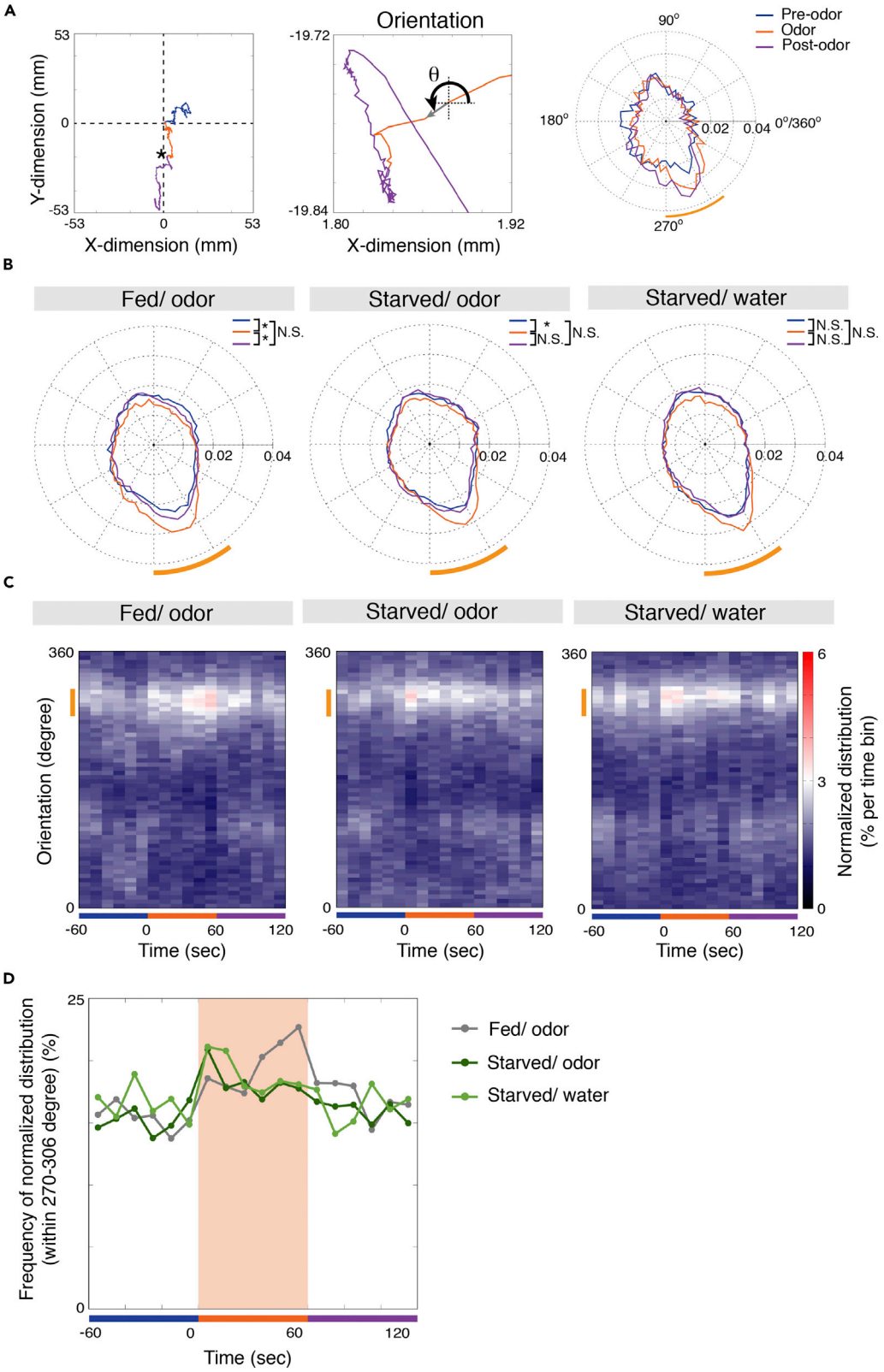
A
Y-dimension (mm)
X-dimension (mm)
Orientation
θ
Pre-odor
Odor
Post-odor
B
Fed/ odor
Starved/ odor
Starved/ water
N.S.
C
Orientation (degree)
Time (sec)
Normalized distribution
(% per time bin)
D
Frequency of normalized distribution
(within 270-306 degree) (%)
Time (sec)
Fed/ odor
Starved/ odor
Starved/ water

Figure 4. Flies with Different Internal States Oriented toward Environmental Cues with Different Temporal Dynamics

(A) Schematic illustrating the calculation of orientation. (Left) A reconstructed walking trajectory. Asterisk indicates the trajectory phase, which is enlarged in the middle panel. (Middle) Orientation is estimated as the counterclockwise angle (black arrow) between the positive x axis (black dashed line) and the vector drawn along the trajectory in a given time interval (gray arrow). (Right) Reconstructed orientation distribution map of a fly during pre-odor (blue), odor (orange), and post-odor (magenta) phases. Radius is the percentage of orientation angles (see Methods). The representative fly tended to orient toward ~288° during odor and post-odor phases. Orange bracket indicates the positional range of the odor source (~270°–306°).

(B) Reconstructed orientation distribution maps from 15 fed flies in response to food odor (left), 16 starved flies in response to food odor (middle), or 17 starved flies in response to water vapor (right) during pre-odor (blue), odor (orange), and post-odor (magenta) phases. Orange brackets indicate the positional range of the odor source (~270°–306°). The percentages of orientation angles derived from flies in the same experimental group and in different odor phases were subjected to statistical analysis (see Methods). Mann-Whitney U test was used to compare the unpaired phases. N.S., not significant. *$p < 0.05$.

(C) Orientation distribution of groups of flies with different internal states (n = 15, 16, and 17 for fed/applied odor, starved/applied odor, and starved/applied water vapor groups, respectively). The orientations of flies were calculated in 10-s time bins. The percentages of orientation distributions of flies in the same group in a given time bin were normalized and shown as heatmap. Orange lines indicate the positional range of the odor source (~270°–306°).

(D) Data were analyzed similar to (C), but only the orientation distribution data in the range between 270° and 306° in (C) were extracted. Each dot represents the normalized frequencies between 270° and 306° of the same group in each time bin.

See also Figures S4 and S5.

food odor, fed flies tended to travel more in straight line, as evidenced by the slight increase in straightness (Figure 5D). Interestingly, the fed flies exhibited reduced straightness soon after the odor was turned off. In contrast, although starved flies also tended to travel more in straight line when they encountered food odor or water, this trend was sustained when the external cues were turned off (Figure 5D).

The rotation of the ball, as evaluated by curl, reflects the behavior of a tethered fly coordinating its six legs to move differentially, rather than walking straight or sideways (Figures 1C and 5E). Notably, curl contains information of magnitude and direction, which includes both positive and negative values that typically cancel each other out when averaged over any appreciable timescale (Figure 5F). Therefore, we focused on only the magnitude, |curl| (Figure 5G). We found that starved flies, but not fed flies, tended to have slightly higher |curl| when they encountered food odor or water (Figure 5G). Interestingly, this trend was only sustained in the post-odor phase for starved flies encountering food odor, but not water vapor. These results collectively suggested that both fed and starved flies tend to walk straighter and/or faster when they encounter environmental cues. Such trends were especially observed in starved flies, which tended to walk much faster when encountering food odor but walked much straighter when encountering water vapor. Interestingly, only starved flies exposed to food odor tended to maintain the walking patterns after the odor was turned off.

The Feature of Ball Rotation Cannot Be Ignored

We next sought to explore how the interplay between distance and curl may reflect the patterns of ball motion and thus fly walking trajectories. We analyzed the cross-correlation between the series of distance and the series of |curl| in 5-s time bins (see Methods). No obvious correlations were found between these two features in any of the three groups for any odor phase (Figure 5H), indicating that |curl| did not shift, either linearly or simultaneously, with changes in distance.

To further understand the interaction between |curl| and distance, we examined the correlation between the average and standard deviation of distance and |curl| in each odor signal phase (Figures 5I and S6). The |curl| value (average) and the changes in |curl| (SD) were both strongly correlated to the distance and changes in distance. These results suggested that the feature distance is only correlated to the feature |curl| (ball rotation) over a short time period (a 5-s time bin), but not at every single sampling time (10 ms).

When the ball rotates along the roll or pitch axis, curl has high correlation with displacement in the X-Y plane. In contrast, when the ball rotates along the yaw axis, curl does not correlate with the displacements along the x and y axes. Therefore, based on our findings that the ball center shifts during experiments (Figures 3G–3I) and the strong correlation between |curl| and distance (Figure 5I), ball rotation is an indispensable feature when reconstructing walking trajectories from the motion of a ball in treadmill systems.

Revisiting the Random Walk of Control Flies

A random walk is mathematically defined as a path or process that is composed of a succession of consistently random steps. Although the biological definition of "random walk" is less clear, the walking patterns

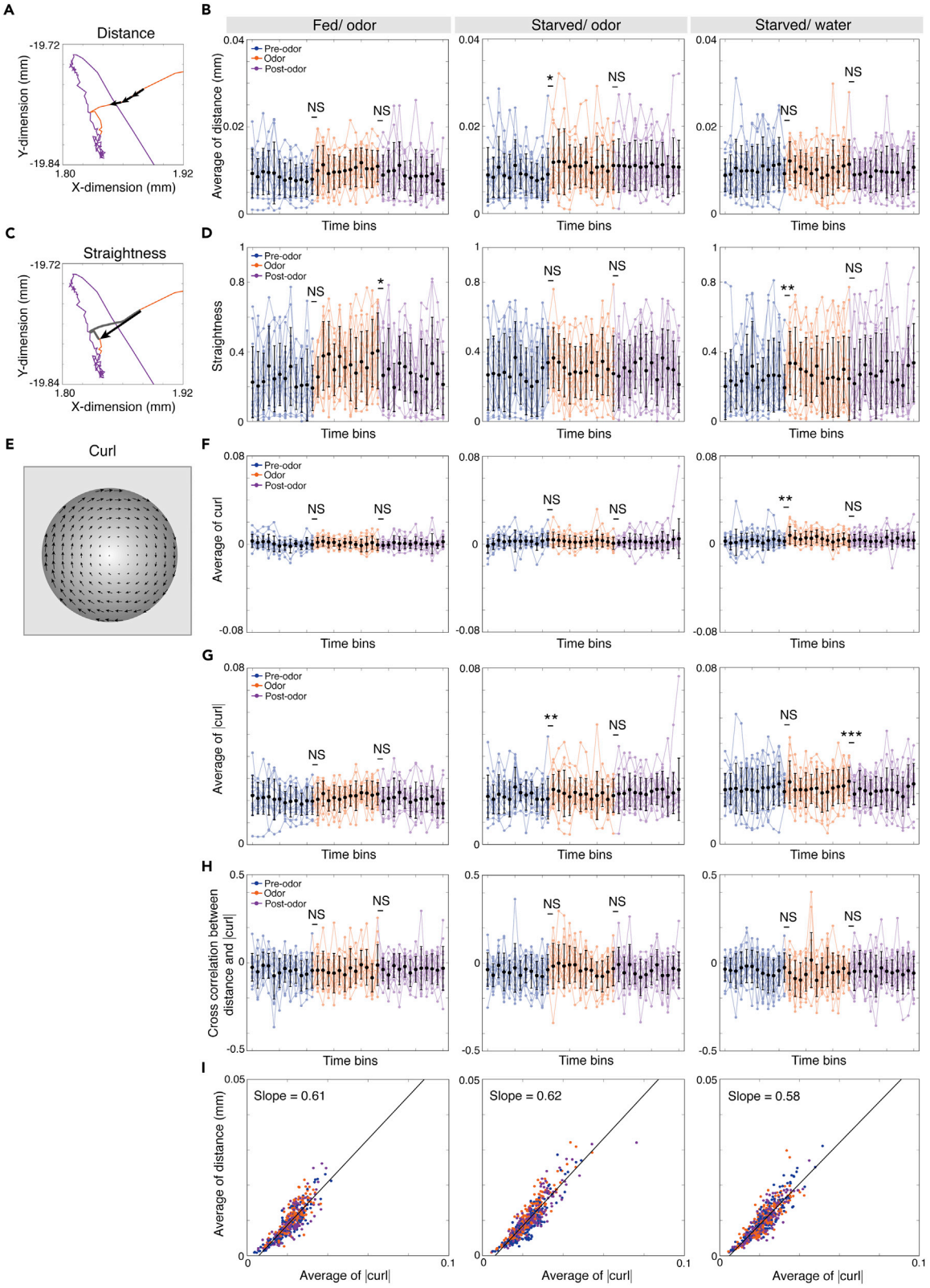
A
Distance
-19.72
-19.84
Y-dimension (mm)
1.80
1.92
X-dimension (mm)
C
Straightness
-19.72
-19.84
Y-dimension (mm)
1.80
1.92
X-dimension (mm)
E
Curl
B
Fed/ odor
Starved/ odor
Starved/ water
Pre-odor
Odor
Post-odor
Average of distance (mm)
0.04
0.02
0
NS
*
Time bins
D
Straightness
1
0.8
0.4
0
**
F
Average of curl
0.08
-0.08
G
Average of |curl|
***
H
Cross correlation between distance and |curl|
0.5
-0.5
I
Slope = 0.61
Slope = 0.62
Slope = 0.58
Average of distance (mm)
0.05
Average of |curl|
0.1

Figure 5. Extracting Walking Features of Flies with Different Internal States

(A) A schematic diagram of distance. Distance (black arrow) is the position change along X- and Y-dimensions between two consecutive 10-ms sampling times.

(B) The average of distance in a given 5-s time bin is shown. Each line represents the average distance traversed by a fly in three odor phases, with same color codes as Figure 1D. The black dots and lines show mean ± SD in each time bin.

(C) A schematic diagram of straightness. Straightness was calculated as the displacement (black arrow)/accumulated distance (gray line) in a 5-s time bin.

(D) The dynamics of straightness in three odor phases. The black dots and lines show mean ± SD in each time bin.

(E) A schematic diagram of curl is shown from the bottom view of the ball. Curl was calculated as the rotation of a displacement field at pixels between two consecutive frames as indicated by arrows.

(F) The curl derived from single flies in each 5-s time bin was averaged. The black dots and lines show mean ± SD in each time bin.

(G) Similar to (F) but shows the absolute value of curl, |curl|.

(H) The cross-correlation between the distance and |curl| was tested in the three groups of flies.

(I) The correlation between average of distance and average of curl in each 5-s time bin derived from three groups of flies.

(B, D, E, G, and H) Mann–Whitney U-test was used to assess paired data for time-binned feature distributions during phase switches. *$p < 0.05$, **$p < 0.01$, ***$p < 0.005$; N.S., not significant. See also Figure S6.

of starved animals under a control environment (without applied cues) are generally described using this term.

We may stipulate that flies were under a control environment before the application of food odor or water vapor, which is the pre-odor phase in our experimental sets. Thus, we reasoned that the features we use to characterize trajectories should allow us to describe the biological random walk of flies, and furthermore we expected that flies with different internal states would differentially perform random walks. We therefore compared the pre-odor phase walking features of fed and starved flies (Figures 6A–6D). We found that starved and fed flies did not exhibit differences in accumulated distance, straightness, frequency of normalized distribution of orientation (within 270°–306°), or accumulated |curl| (Figure 6C). The 28 variables extracted from the walking patterns of fed and starved flies were then subjected to principle-component analysis (PCA) to test whether these variables can collectively distinguish between the walking patterns of fed and starved flies (Figures 6D and S7). We did not observe clear separation of the two clusters, suggesting that fed and starved flies may have similar walking patterns when there was no obvious external cue.

Lévy walk and Lévy flight, two types of scale-free behavior, are the best-established analyses to describe the "random walk/flight" of animal search strategies (Rhee et al., 2011; Bartumeus et al., 2005; Reynolds and Frye, 2007). The distribution of velocity patterns for Brownian motion exhibits a normal distribution, whereas that of scale-free movement is not normal; instead, it is characterized by a fat tail or self-similarity (Mörters and Peres, 2010; Clauset et al., 2009). To further address whether flies walked in a scale-free manner or as a random walk without application of external cues, we subjected the features of distance, change of orientation, and change of curl to scale-free analysis (Figures 6E and 6F). This analysis involves calculating the power-law scaling α from the structure functions for displacements ΔX_T over sampling time T. When the power-law scaling $\alpha < 0.5$, the movement of subjects is considered to be odd. When α approximates 0.5, the subject movement is considered to be a random walk. When $\alpha > 0.5$, the walking patterns are considered to be scale free, as they follow a power-law function (Figure 6E). We found that fed and starved flies both exhibited scale-free patterns for all three tested features (Figure 6F).

After calculating orientation, distance, straightness and curl to characterize the walking features of a fly recorded by the treadmill system, we sought to test whether these features are collectively sufficient to identify differential walking strategies. We plotted the changes of orientation and curl along the cumulative distance for each of the three odor signal phases (Figures 6G and S8). Indeed, these features clearly reflected the differential walking patterns or strategies employed by flies with different internal states and encountering different environmental cues.

DISCUSSION

Treadmill systems have been widely employed to monitor animal walking trajectories and to dissect neural mechanisms in subjects that are performing assigned tasks. The most prevalent treadmill systems used for mammals and insects are computer-mouse-mode systems that have the advantage of a fast closed feedback loop but lack focus verification and information about rotation index. To bypass these two issues, we built an easily adapted camera-mode treadmill system and identified a set of features that sufficiently describe fly walking trajectories. We further demonstrated the power of this system by decoding the

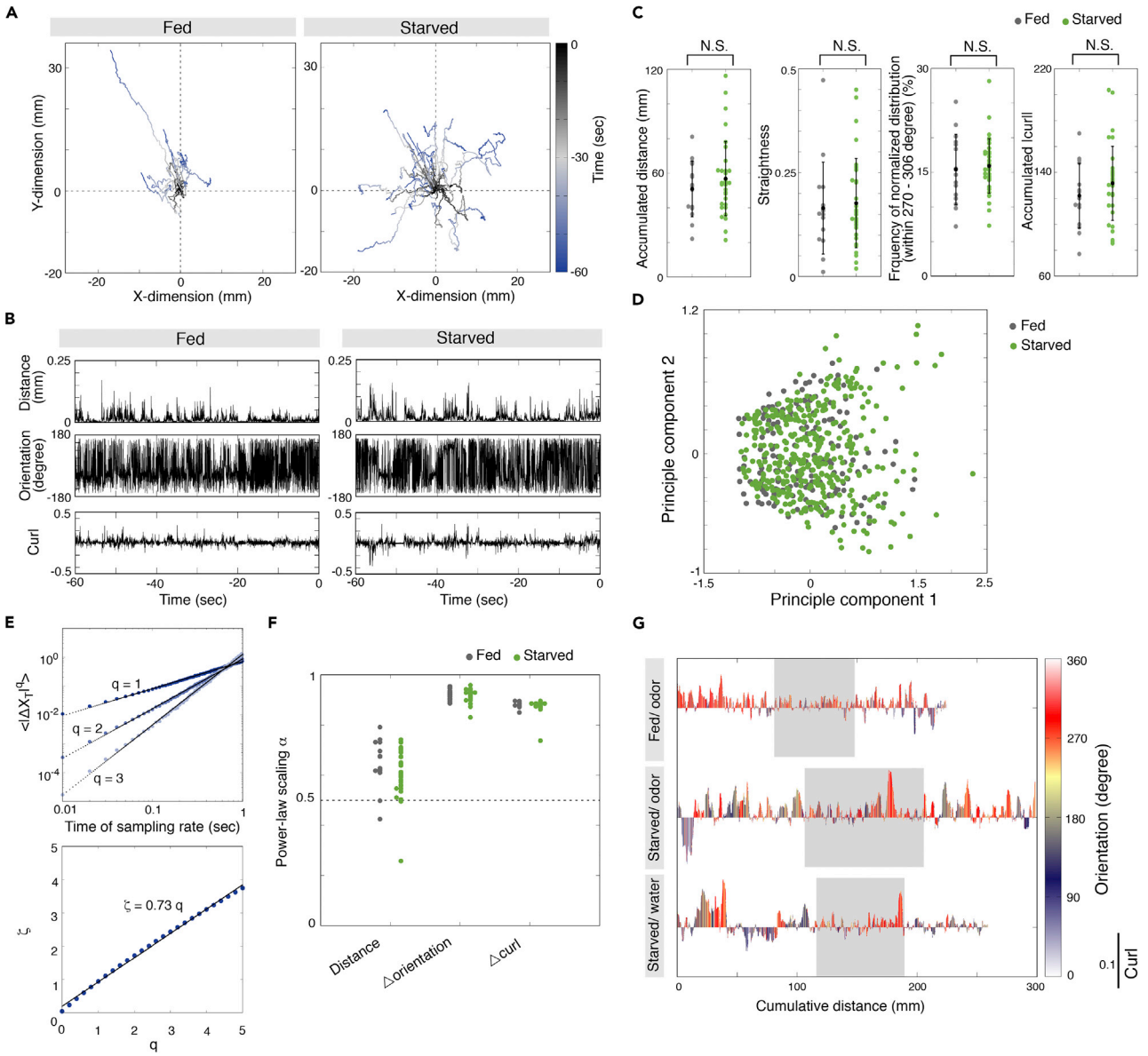

Figure 6. Flies with Different Internal States Showed Similar Scale-free Walking Patterns

(A) The reconstructed walking trajectories of fed (left panel, n = 15) or starved (right panel, n = 33) flies in the pre-odor phase. The trajectories are coded blue (start) to black (end) as indicated.

(B) The features of a single fed (left) or a single starved (right) fly.

(C) Accumulated distance, straightness, frequency of normalized distribution of orientation within 270°–306°, and accumulated |curl| of fed and starved flies. The black dots and lines show mean ± SD in each group. Mann-Whitney U test to compare the unpaired phases. N.S., not significant.

(D) Principle-component analysis of 28 features derived from the fed and starved fly walking patterns in the pre-odor phase.

(E) A representative scale-free analysis of a starved fly walking trajectories in the pre-odor phase. Power-scaling ζ was calculated from least-squares linear fitting of the structure functions showing displacements ΔX_T in an increased sampling time T on a log-log plot (top). The power-law scaling α was obtained by least-squares linear fitting of the power-scaling ζ against the power q (bottom) (Methods). In this case, the power-law scaling α = 0.73.

(F) The power-law scaling for distance, Δorientation, and Δcurl derived from fed and starved flies in the pre-odor phase.

(G) Representative trials from three flies with different internal states and encountered different environmental cues. The dynamics of three walking features, curl, orientation, and accumulated displacement are shown throughout the three phases. Representative data from flies in the three groups are shown. The odor-phase is indicated by the gray shadow. The y axis shows the value of curl (positive and negative values represent two opposite rotation directions). Orientation is color coded as shown. Scale bar for curl, 0.1.

See also Figures S7 and S8.

differential walking strategies that reflect the internal states of animals. The major difference in output between our system and those equipped with two-chip sensors is that the yaw, pitch, and roll of ball motion are derived from the X and Y displacements, respectively, detected by two chips in those mouse-mode treadmills, but ours directly measures the rotation and curl of ball motion. Moreover, unlike previous camera-mode treadmill, a pre-established ball pattern model is not required by our system. Importantly, the system described here can also be scaled up for application to other animal species.

The Camera-Mode Treadmill System

Our camera-mode treadmill system has several advantages. First, the float mount is equipped with four airflow inlets to support the ball, which largely eliminated the frequent problem of air turbulence when using a single airflow inlet; thus, our system is amenable to long-term recording. Second, camera-based video recording combined with frame-by-frame signal translation by optical flow allows for verification of reconstructed trajectories. Third, a set of features, including curl from ball rotation, effectively describes the trajectory patterns. In addition, the estimation of odor arrival delay time with a PID improves the accuracy of measuring dynamic trajectory pattern responses to odor administration.

We assembled a set of features to describe the reconstructed walking trajectories: distance, straightness, orientation, and curl (Figures 4 and 5). These four features have enough power to describe the different walking patterns of flies with different internal states and encountering different external cues. Most importantly, we found that curl is highly correlated with distance, which means that this parameter is indispensable when analyzing X- and Y-displacement (also see below discussion) (Figures 5I and S6). Distance and straightness are the products of ball motion along an X-Y plane, whereas |curl| is derived from the rotation of the ball. All these three features collaboratively reflect the movement of a fly. Accordingly, we may further envision the combination of standard deviation of curl and the average of displacement as the product of fly walking speed. Therefore, our results suggest that the faster a fly walks on the ball, the more dynamic (variable) the ball rotation is. Our findings further support the idea that curl can serve as a biologically meaningful feature of fly walking behavior that can be measured by treadmill systems. Specifically, when curl is calculated over a very short sampling time (e.g., millisecond scale), it may reflect changes in fly stepping patterns. On the other hand, when the sample time is on the scale of seconds, curl may instead reflect effects on guidance strategies.

Ball Rotation and Curl

The computer-mouse-mode treadmill systems used for flies, mice, and rats lack the capacity to detect ball rotation and/or shift of the rotation center. It is not clear how this information deficit may affect the reconstructed walking trajectories. However, using our camera-mode treadmill system, we found the ball rotation centers frequently shifted during experimental phases (Figures 2D, 2E, and 3G–3I). Such rotation center drift demonstrated that the ball often switched its rotation along yaw, roll, or pitch axes. Therefore, reconstructing the trajectories through two orthogonally aligned mouse cameras may result in under- or over-estimated distances. To better understand the relationship between ball rotation and reconstructed distance, we calculated curl to quantify ball rotation along time. We found that the average and standard deviation of |curl| are highly correlated with the average and standard deviation of distance (Figures 5I and S6). Therefore, the ball rotation feature cannot be ignored when reconstructing animal walking trajectories.

Internal State-Dependent Walking Strategies

A growing body of evidence has demonstrated that inner conditions and past experiences contribute to motivation and decision-making mechanisms that guide animal behavior in response to environmental cues (Kim and Dickinson, 2017; Rengarajan et al., 2019; Jennings et al., 2019). Flies in different physical conditions may have different motivation levels and sensitivity to environmental cues, depending on the correspondence between these cues and their internal states. We therefore applied either food odor or water vapor to fed or starved flies and monitored their walking trajectories during different odor phases to test the performance of the four features of trajectory that we analyzed.

Starved flies oriented themselves toward the external cues more quickly than fed flies, irrespective of whether the cue was food odor or water vapor (Figures 4C and 4D). This result implies that starved flies may be more attentive to environmental cues than fed flies. Interestingly, as soon as the food odor was turned off, fed flies immediately returned to walking patterns with shorter distance or lower speed, whereas starved flies continued to walk with longer distance or higher speed (Figure 5B). Differential post-odor

behaviors were also found in the average of |curl| for starved flies. When the odor supply was turned off, starved flies experiencing food odor maintained the higher average of |curl|, whereas in starved flies experiencing water vapor, this feature immediately dropped to a level similar to that in the pre-odor phase (Figure 5G). These results suggest that starved and fed flies exhibit different post-experience behaviors.

Because the PCA did not show obvious clustering of different experimental groups or odor phases, it may be that 28 walking variables are not sufficient to discriminate groups or phases in the eigenspace. This insufficiency could result from minor differences in walking features among the test subjects. Collectively, the four features of rotation, distance, straightness, and curl have enough power to distinguish the internal status-dependent behaviors both during and after the administration of cues.

Random Walk Revisited

Starved flies have been broadly used as controls in many experimental paradigms; however, this internal state clearly biases the decision making that determines walking patterns. We therefore revisited the idea that control flies perform a random walk. We did not observe significant differences between fed and starved flies in any examined baseline features or analyses (Figure 6). Thus, our results offer support to the notion that fed and starved flies do not show significant differences in walking patterns when there is no obvious external cue. However, we cannot exclude the possibility that the analytic tools used in this work do not have sufficient power to identify subtle differences.

The fundamental difference between Brownian motion and scale-free movement is in the distribution of velocity patterns: Brownian motion has a normal distribution, whereas scale-free motion has a non-normal distribution. Moreover, scale-free movement may exhibit strong correlation between events along time, which is not a feature of Brownian motion. Therefore, such scale-free walking trajectories may reflect the existence of a "mind" or "thinking" (Raichlen et al., 2014). Interestingly, we noticed that the correlation between |curl| and distance existed over short time periods (Figures 5I and S6) and not at every single sampling time (Figure 5H). This observation indicated that the correlation was not derived from simultaneous fluctuations of distance and |curl| but from their global tendencies. In the future, it will be interesting to explore possible relationship between the global tendencies of distance and |curl| and the event correlation properties of scale-free movement.

Limitations of the Study

Although the current camera-mode treadmill system solves some problems with computer-mouse-mode treadmill systems, the build reported herein did not offer fast-enough feedback signals to reconstruct trajectories in real time. In the future, faster frame capture and transmission may overcome this limitation. In addition, we did not simultaneously record the gait or movements of the six legs on each tested fly while it was walking on the ball. This lack of information made correlating the individual features of ball motion to any aspect of fly movement infeasible. In the future, simultaneous recording of the fly and the ball (Kain et al., 2013) will solve this issue.

METHODS

All methods can be found in the accompanying Transparent Methods supplemental file.

DATA AND CODE AVAILABILITY

The original, unprocessed data and script used in this study will be available upon request.

SUPPLEMENTAL INFORMATION

Supplemental Information can be found online at https://doi.org/10.1016/j.isci.2019.08.054.

ACKNOWLEDGMENTS

We thank Drs. Daisuke Yamamoto and Soh Kohatsu for sharing the original designs of treadmill system, Wen-Liang Hwang for insightful suggestion of optic flow, Thomas Clandinin for Oregon R fly, and Michael Dickinson for sharing wild-caught flies. We thank Mr. Hsin Chu Chen (Taiwan Instrument, Taiwan) for manufacturing the first version of float mount (v1) and High Precision Machine Shop (Institute of Physics, Academia Sinica) for manufacturing later versions of float mounts (v2 and v3). We thank reviewers for their

insightful comments, which helped us clarify some interpretations. We thank Dr. Marcus Calkins and members of Chou's laboratory for feedback, especially Chi-Jen Yang and Nan-Fu Liou. K.-T.T. is an Academia Sinica Regular Postdoctoral Scholar. This work was supported by a Career Development Award (AS-102-CDA-L02) to Y.-H.C.

AUTHOR CONTRIBUTIONS

Y.-H.C initiated the idea and project. K.-T.T and Y.-H.C. designed experiments. K.-T.T. built the treadmill system and odor delivery system, with feedback from Y.-H.C. K.-T.T. collected and analyzed data and wrote scripts. Y.-H.C. supervised the project. Y.-H.C and K.-T.T. wrote the manuscript.

DECLARATION OF INTERESTS

The authors declare no competing interests.

Received: July 2, 2019
Revised: August 18, 2019
Accepted: August 27, 2019
Published: September 27, 2019

REFERENCES

Álvarez-Salvado, E., Licata, A.M., Connor, E.G., Mchugh, M.K., King, B.M.N., Stavropoulos, N., Victor, J.D., Crimaldi, J.P., and Nagel, K.I. (2018). Elementary sensory-motor transformations underlying olfactory navigation in walking fruit-flies. Elife *7*, e37815.

Anderson, D.J., and Perona, P. (2014). Toward a science of computational ethology. Neuron *84*, 18–31.

Bahl, A., Ammer, G., Schilling, T., and Borst, A. (2013). Object tracking in motion-blind flies. Nat. Neurosci. *16*, 730.

Bahl, A., Serbe, E., Meier, M., Ammer, G., and Borst, A. (2015). Neural mechanisms for Drosophila contrast vision. Neuron *88*, 1240–1252.

Bartumeus, F., Da Luz, M.G.E., Viswanathan, G.M., and Catalan, J. (2005). Animal search strategies: a quantitative random-walk analysis. Ecology *86*, 3078–3087.

Bidaye, S.S., Machacek, C., Wu, Y., and Dickson, B.J. (2014). Neuronal control of Drosophila walking direction. Science *344*, 97–101.

Borst, A., and Heisenberg, M. (1982). Osmotropotaxis in Drosophila melanogaster. J. Comp. Physiol. *147*, 479–484.

Branson, K., Robie, A.A., Bender, J., Perona, P., and Dickinson, M.H. (2009). High-throughput ethomics in large groups of Drosophila. Nat. Methods *6*, 451.

Buchner, E. (1976). Elementary movement detectors in an insect visual system. Biol. Cybernetics *24*, 85–101.

Clark, D.A., Bursztyn, L., Horowitz, M.A., Schnitzer, M.J., and Clandinin, T.R. (2011). Defining the computational structure of the motion detector in Drosophila. Neuron *70*, 1165–1177.

Clauset, A., Shalizi, C.R., and Newman, M.E.J. (2009). Power-law distributions in empirical data. SIAM Rev. *51*, 661–703.

Coen, P., Clemens, J., Weinstein, A.J., Pacheco, D.A., Deng, Y., and Murthy, M. (2014). Dynamic sensory cues shape song structure in Drosophila. Nature *507*, 233.

Dankert, H., Wang, L., Hoopfer, E.D., Anderson, D.J., and Perona, P. (2009). Automated monitoring and analysis of social behavior in Drosophila. Nat. Methods *6*, 297.

Dickinson, M.H., Farley, C.T., Full, R.J., Koehl, M.A., Kram, R., and Lehman, S. (2000). How animals move: an integrative view. Science *288*, 100–106.

Gaudry, Q., Hong, E.J., Kain, J., De Bivort, B.L., and Wilson, R.I. (2012a). Asymmetric neurotransmitter release enables rapid odour lateralization in Drosophila. Nature *493*, 424.

Gaudry, Q., Nagel, K.I., and Wilson, R.I. (2012b). Smelling on the fly: sensory cues and strategies for olfactory navigation in Drosophila. Curr. Opin. Neurobiol. *22*, 216–222.

Gomez-Marin, A., Stephens, G.J., and Louis, M. (2011). Active sampling and decision making in Drosophila chemotaxis. Nat. Commun. *2*, 441.

Greenspan, R.J., and Ferveur, J.-F. (2000). Courtship in drosophila. Annu. Rev. Genet. *34*, 205–232.

Grover, D., Katsuki, T., and Greenspan, R.J. (2016). Flyception: imaging brain activity in freely walking fruit flies. Nat. Methods *13*, 569.

Grunwald Kadow, I.C. (2019). State-dependent plasticity of innate behavior in fruit flies. Curr. Opin. Neurobiol. *54*, 60–65.

Haberkern, H., Basnak, M.A., Ahanonu, B., Schauder, D., Cohen, J.D., Bolstad, M., Bruns, C., and Jayaraman, V. (2019). Visually guided behavior and optogenetically induced learning in head-fixed flies exploring a virtual landscape. Curr. Biol. *29*, 1647–1659.e8.

Harvey, C.D., Collman, F., Dombeck, D.A., and Tank, D.W. (2009). Intracellular dynamics of hippocampal place cells during virtual navigation. Nature *461*, 941.

Jennings, J.H., Kim, C.K., Marshel, J.H., Raffiee, M., Ye, L., Quirin, S., Pak, S., Ramakrishnan, C., and Deisseroth, K. (2019). Interacting neural ensembles in orbitofrontal cortex for social and feeding behaviour. Nature *565*, 645–649.

Kabra, M., Robie, A.A., Rivera-Alba, M., Branson, S., and Branson, K. (2012). JAABA: interactive machine learning for automatic annotation of animal behavior. Nat. Methods *10*, 64.

Kain, J., Stokes, C., Gaudry, Q., Song, X., Foley, J., Wilson, R., and De Bivort, B. (2013). Leg-tracking and automated behavioural classification in Drosophila. Nat. Commun. *4*, 1910.

Kim, I.S., and Dickinson, M.H. (2017). Idiothetic path integration in the fruit fly Drosophila melanogaster. Curr. Biol. *27*, 2227–2238.e3.

Klafter, J., Shlesinger, M.F., and Zumofen, G. (1996). Beyond brownian motion. Phys. Today *49*, 33.

Kohatsu, S., Koganezawa, M., and Yamamoto, D. (2011). Female contact activates male-specific interneurons that trigger stereotypic courtship behavior in Drosophila. Neuron *69*, 498–508.

Kohatsu, S., and Yamamoto, D. (2015). Visually induced initiation of Drosophila innate courtship-like following pursuit is mediated by central excitatory state. Nat. Commun. *6*, 6457.

Lehnert, B.P., Baker, A.E., Gaudry, Q., Chiang, A.S., and Wilson, R.I. (2013). Distinct roles of TRP channels in auditory transduction and amplification in Drosophila. Neuron *77*, 115–128.

Moore, R.J.D., Taylor, G.J., Paulk, A.C., Pearson, T., Van Swinderen, B., and Srinivasan, M.V. (2014). Fictrac: a visual method for tracking spherical

motion and generating fictive animal paths. J. Neurosci. Methods *225*, 106–119.

Mörters, P., and Peres, Y. (2010). Brownian Motion (Cambridge University Press).

Radvansky, B.A., and Dombeck, D.A. (2018). An olfactory virtual reality system for mice. Nat. Commun. *9*, 839.

Raichlen, D.A., Wood, B.M., Gordon, A.D., Mabulla, A.Z.P., Marlowe, F.W., and Pontzer, H. (2014). Evidence of Levy walk foraging patterns in human hunter-gatherers. Proc. Natl. Acad. Sci. U S A *111*, 728–733.

Rengarajan, S., Yankura, K.A., Guillermin, M.L., Fung, W., and Hallem, E.A. (2019). Feeding state sculpts a circuit for sensory valence in Caenorhabditis elegans. Proc. Natl. Acad. Sci. U S A *116*, 1776–1781.

Reynolds, A.M., and Frye, M.A. (2007). Free-flight odor tracking in Drosophila is consistent with an optimal intermittent scale-free search. PLoS One *2*, e354.

Rhee, I., Shin, M., Hong, S., Lee, K., Kim, S.J., and Chong, S. (2011). On the Levy-walk nature of human mobility. IEEE/ACM Trans. Networking *19*, 630–643.

Ribeiro, I.M.A., Drews, M., Bahl, A., Machacek, C., Borst, A., and Dickson, B.J. (2018). Visual projection neurons mediating directed courtship in Drosophila. Cell *174*, 607–621.e18.

Robie, A.A., Hirokawa, J., Edwards, A.W., Umayam, L.A., Lee, A., Phillips, M.L., Card, G.M., Korff, W., Rubin, G.M., Simpson, J.H., et al. (2017). Mapping the neural substrates of behavior. Cell *170*, 393–406.e28.

Runyan, C.A., Piasini, E., Panzeri, S., and Harvey, C.D. (2017). Distinct timescales of population coding across cortex. Nature *548*, 92.

Sato, M., Kawano, M., Mizuta, K., Islam, T., Lee, M.G., and Hayashi, Y. (2017). Hippocampus-dependent goal localization by head-fixed mice in virtual reality. eNeuro *4*, ENEURO.0369-16.2017.

Seelig, J.D., Chiappe, M.E., Lott, G.K., Dutta, A., Osborne, J.E., Reiser, M.B., and Jayaraman, V. (2010). Two-photon calcium imaging from head-fixed Drosophila during optomotor walking behavior. Nat. Methods *7*, 535.

Semmelhack, J.L., and Wang, J.W. (2009). Select Drosophila glomeruli mediate innate olfactory attraction and aversion. Nature *459*, 218.

Takasaki, T., Namiki, S., and Kanzaki, R. (2012). Use of bilateral information to determine the walking direction during orientation to a pheromone source in the silkmoth Bombyx mori. J. Comp. Physiol. A *198*, 295–307.

Van Breugel, F., Huda, A., and Dickinson, M.H. (2018). Distinct activity-gated pathways mediate attraction and aversion to CO2 in Drosophila. Nature *564*, 420–424.

Wu, M.-C., Chu, L.-A., Hsiao, P.-Y., Lin, Y.-Y., Chi, C.-C., Liu, T.-H., Fu, C.-C., and Chiang, A.-S. (2014). Optogenetic control of selective neural activity in multiple freely moving Drosophila adults. Proc. Natl. Acad. Sci. U S A *111*, 5367–5372.

Zhou, Y., and Wilson, R.I. (2012). Transduction in Drosophila olfactory receptor neurons is invariant to air speed. J. Neurophysiol. *108*, 2051–2059.

ISCI, Volume *19*

Supplemental Information

Random Walk Revisited: Quantification and Comparative Analysis of *Drosophila* Walking Trajectories

Kuo-Ting Tsai and Ya-Hui Chou

Supplemental Figures

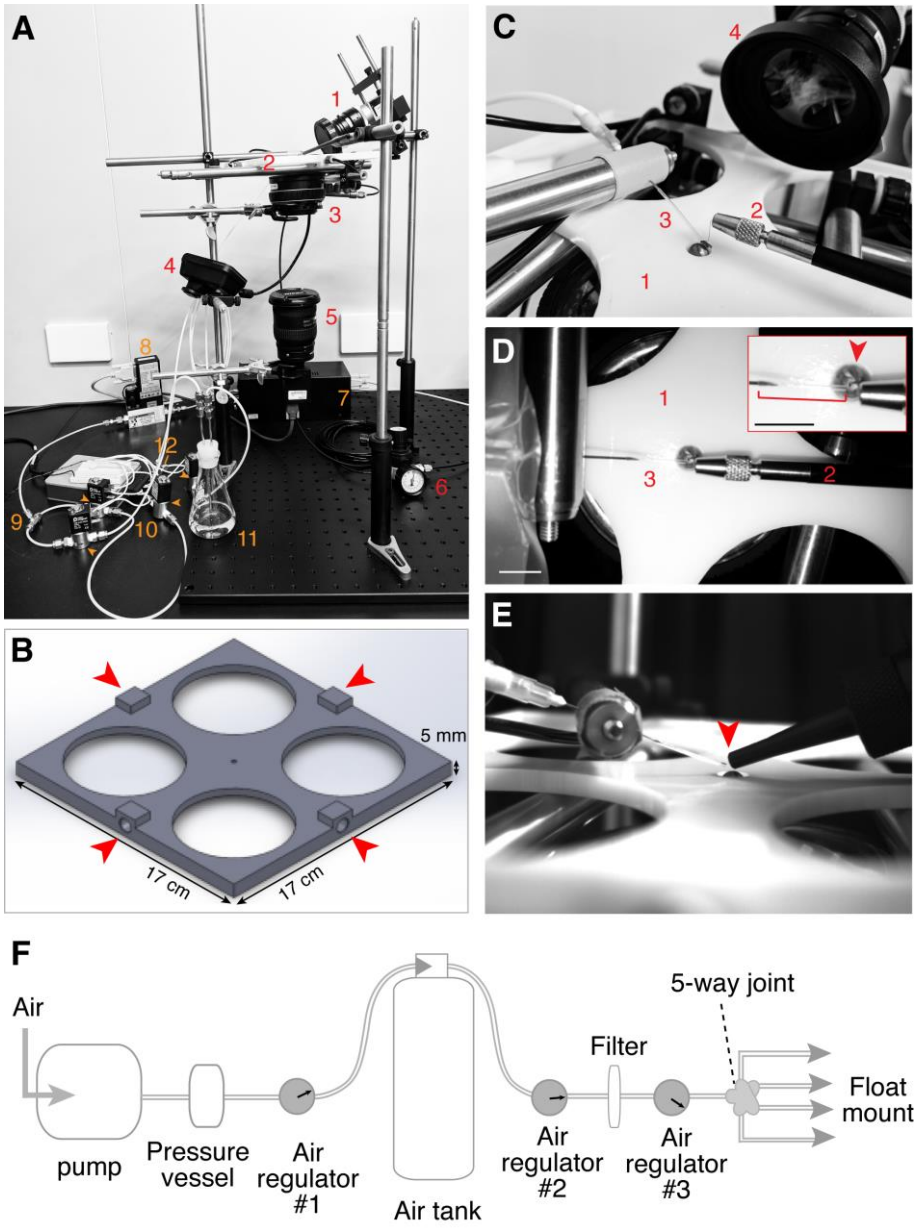

Figure S1. The settings of fly treadmill (Related to Figure 1)

(A) Photograph of the camera-mode treadmill system. 1, high speed CCD camera (#2); 2, float mount; 3, infrared LED illuminator; 4, controller for infrared LED illuminator; 5, high speed CCD camera (#1); 6, controller for air pump; 7, flowmeter supplier; 8, mass flow meter; 9, 3-way joint #1; 10, four sets of 2-way solenoid valves (arrowheads); 11, flask with odor and/or water; 12, 3-way joint #2. The schematic diagrams of treadmill system (items in red) and odor delivery system (items in orange) can be found in Figure 1A and Figure S2A, respectively. (B) Schematic of float mount. Arrowheads indicate the inlets of air streams. (C, D) 1, float mount; 2, fly tether; 3, tip of nozzle; 4, high speed CCD camera (#2). (C) Lateral view of float mount shows a tethered fly. An enlargement of the image is shown in Figure 1B. (D) Top view of float mount shows a tethered fly. Inset shows the odor-delivery needle (nozzle) with a 1.5-cm disposable polyethylene end tube (bracket). Arrowhead indicates the ball. Scale bars, 1 cm. (E) A photoionization detector (PID) is located at the detector tip (arrowhead) in the position of a tethered fly. (F) The schematic diagram of air pipeline to the float mount (see Methods).

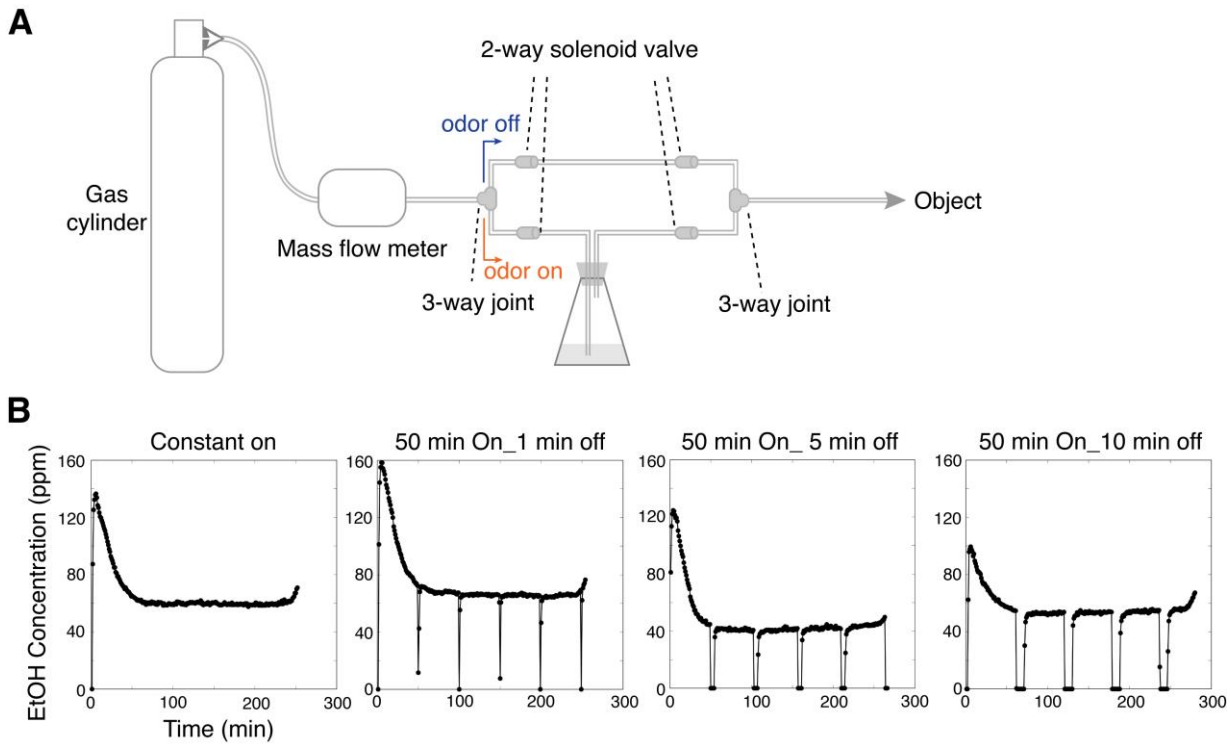

Figure S2. The odor delivery system (Related to Figure 1)

(A) Schematic of the odor delivery system. The air was 21% O_2 and 79% N_2. (B) The efficacy of PID and 2-way solenoid system. The dynamics of odor concentrations were monitored when saturated EtOH was flowed under the control of on-off 2-way solenoid system with: constant on, 50-min on and 1-min off, with 50-min on and 5-min off, or with 50-min on and 10-min off (from left to right). The concentration of odor flow released from the nozzle was monitored real-time by PID when 10 ml absolute EtOH was flowed by 10 mL/min airflow. The odor delivery reached a steady state after 60 min, which reflects the accumulation time of saturated EtOH in the delivery system. The odor concentration signal was elevated at around 235 min, which reflects the time at which the PID battery ran down.

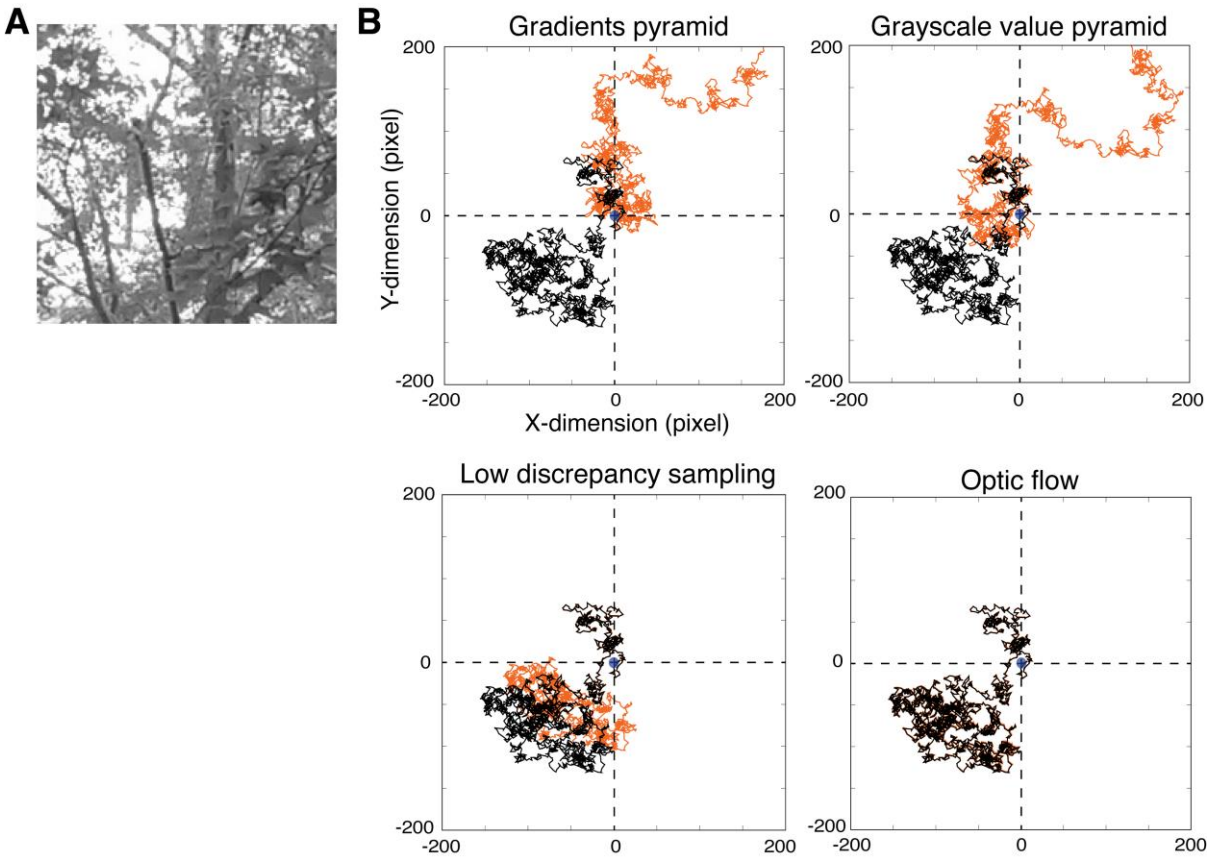

Figure S3. Translation of object motion in serial frames to a trajectory (Related to Figure 2)

(A) A single frame of tested video (200 pixels x 200 pixels) (Supplementary Movie 2). The photo moves based on the trajectory (real trajectory in B). (B) Comparisons of the trajectories constructed through four different methods (Gradient pyramid, Grayscale value pyramid, Low discrepancy sampling, and optic flow; orange) and the real trajectory (black). The trajectory reconstructed by optic flow best recaptures the real trajectory. (See also video S2.)

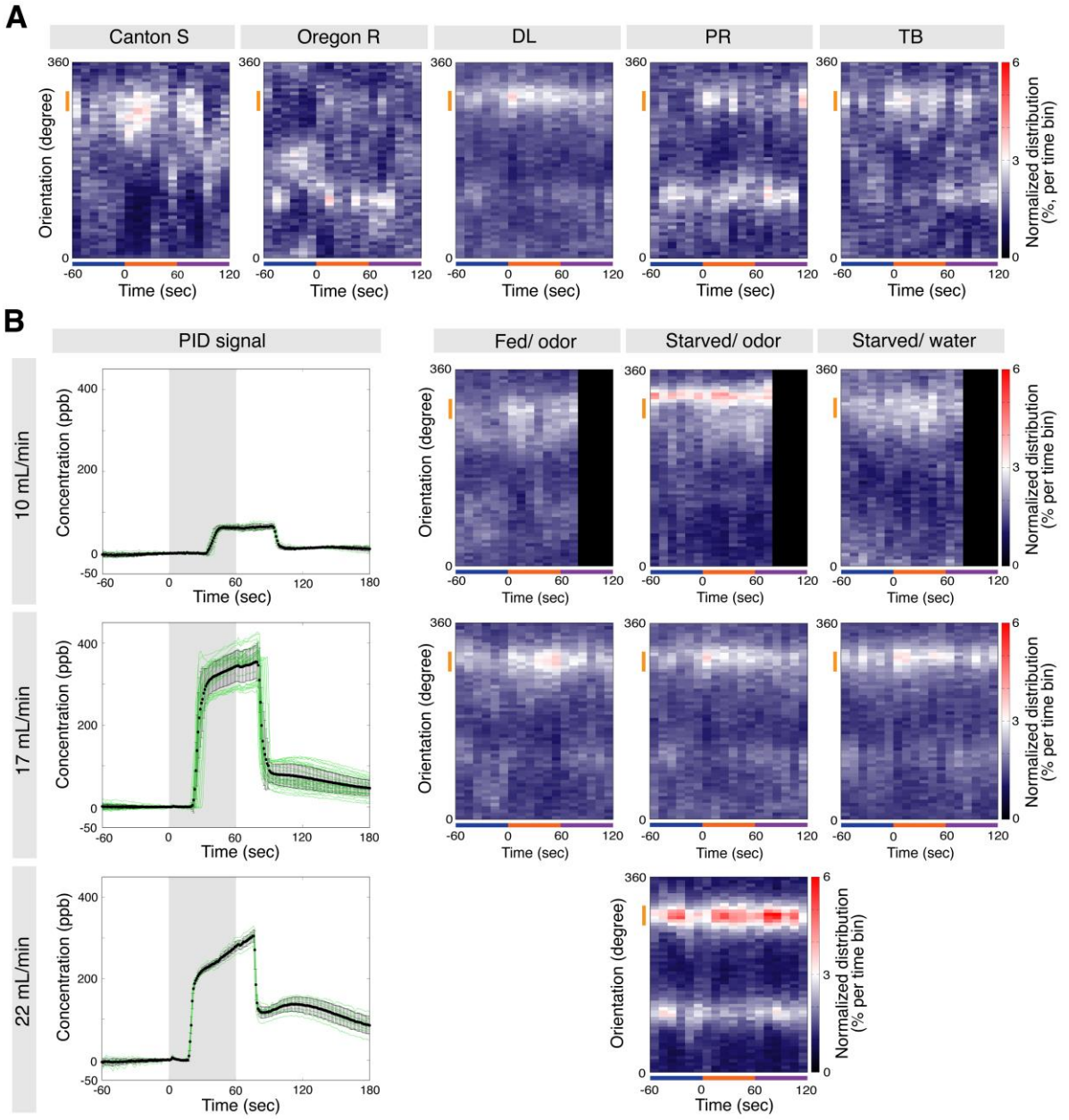

Figure S4. The responses of different wild-type strains of flies to odor (Related to Figure 4)

(A) Orientation distribution of five wild-type strains of starved flies in response to a 10^{-1} dilution of pentanoic acid (17 mL/min). Similar to Figure 4C, the orientations of flies were calculated in 10-sec time bins. The orientation distributions of flies in the same group in a given time bin were normalized and shown as a heat-map. Note that DL flies show more consistent orientation dynamics in the three odor-phases. The number in each group was 5 (Canton S), 5 (Oregon R), 16 (DL), 6 (PR) and 6 (TB) flies. Orange lines indicate the positional range of the odor source (~270°-306°).

(B) (Left) The PID signal in three solenoid on-off phases under three different flow rates are shown as in Figure 1D. The mean delay time was 34 sec, 22 sec, and 18 sec for odor plume delivery at 10 mL/min, 17 mL/min and 22 mL/min, respectively. Black lines indicate the average of 7, 29, or 8 trials (green lines) for 10, 17 and 22 mL/min, respectively, and are shown as mean ± S.D. (Middle to right) The orientations of flies with different internal states toward odor or water vapors delivered through three different flow rates. The results in pre-odor, odor and post-odor phases were calibrated based on the PID signals. The number in each group was 14, 11, and 10 (Top row, left to right), 15, 16, and 17 (middle row, left to right) and 10 (bottom row). The PID and orientation distribution at 17 mL/min are the same as shown in Fig. 1D and 4C, respectively. Orange lines indicate the positional range of the odor source (~270°-306°).

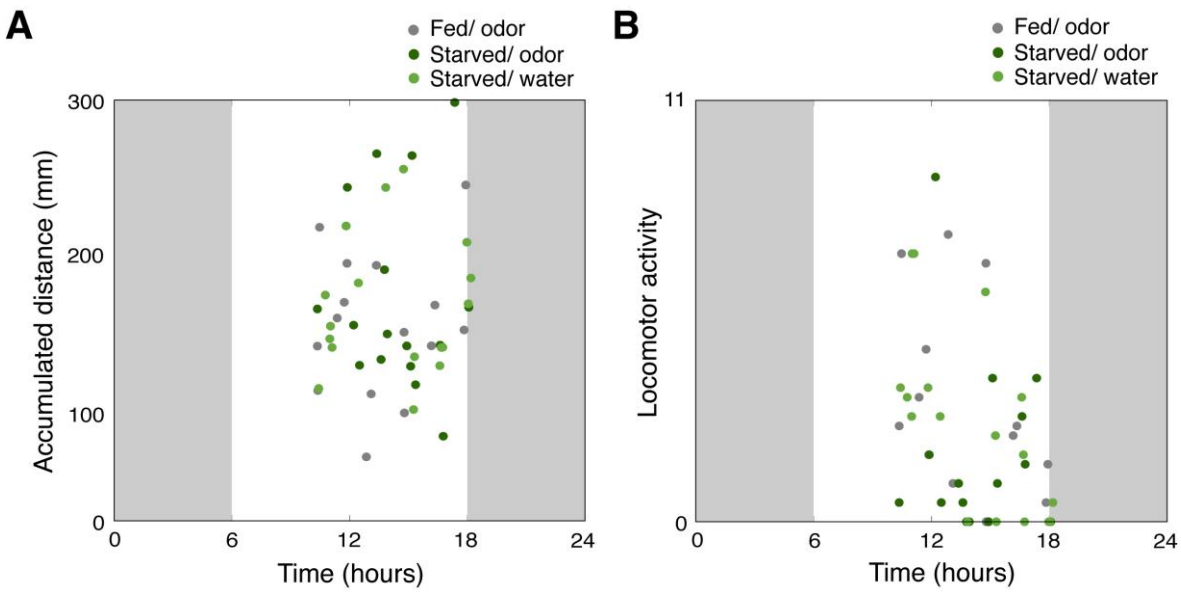

Figure S5. Flies with different internal states have no obvious circadian-dependent effects during day on the response to odor or water vapor (Related to Figure 4)

(A) The accumulated distances of flies are independent to the data acquisition time. The day and night cycle is shaded in white and grey, respectively. Each dot represents the data of an individual fed fly in response to odor (grey), starved fly in response to odor (green) or starved flies in response to water vapor (light green). (B) Similar to (A), but each dot represents the locomotor activity of a fly. Starved flies (green and light green) did not show obvious locomotor activity differences compared to fed flies (grey).

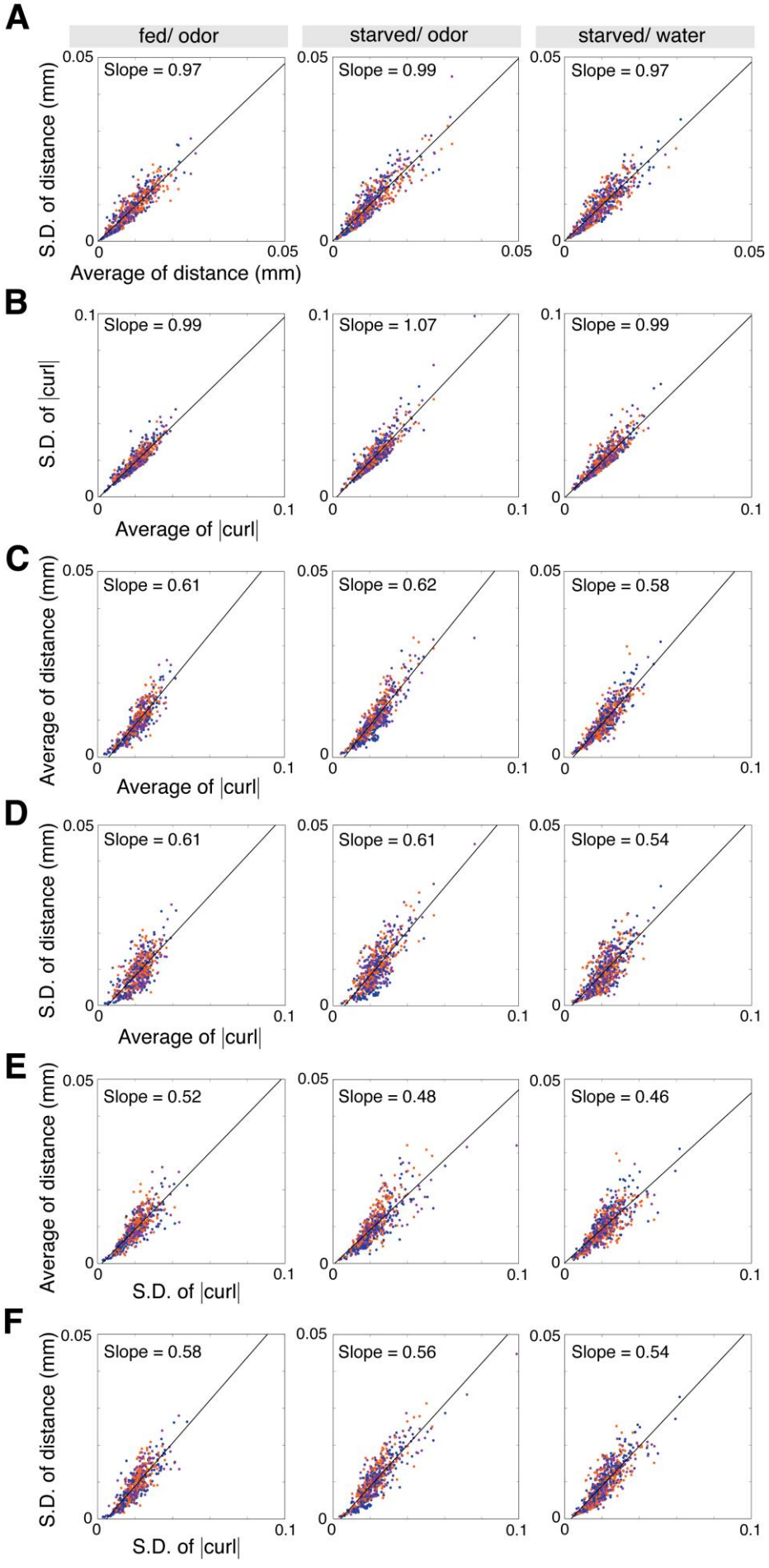
A
fed/ odor
starved/ odor
starved/ water
S.D. of distance (mm)
Average of distance (mm)
Slope = 0.97
Slope = 0.99
Slope = 0.97
B
S.D. of |curl|
Average of |curl|
Slope = 0.99
Slope = 1.07
Slope = 0.99
C
Average of distance (mm)
Average of |curl|
Slope = 0.61
Slope = 0.62
Slope = 0.58
D
S.D. of distance (mm)
Average of |curl|
Slope = 0.61
Slope = 0.61
Slope = 0.54
E
Average of distance (mm)
S.D. of |curl|
Slope = 0.52
Slope = 0.48
Slope = 0.46
F
S.D. of distance (mm)
S.D. of |curl|
Slope = 0.58
Slope = 0.56
Slope = 0.54
0
0.05
0.1

Figure S6. The correlation between distance and |curl| (Related to Figure 5)

(A) The correlation between average of distance and S.D. of distance. Each dot represents the average distance and S.D. of distance from a given fly in a given 5-sec time bin. The dots were color-coded to indicate pre-odor (blue), odor (orange) and post-odor (magenta) phases.
(B) Similar to (A) but shows the correlation between average of |curl| and S.D. of |curl|.
(C-F) Similar to (A) but shows the correlations between average of distance and average of |curl| (C), S.D. of distance and average of |curl| (D), average of distance and S.D. of |curl| (E), or S.D. of distance and S.D. of |curl| (F). (C) is the same as those shown in Figure 5I.

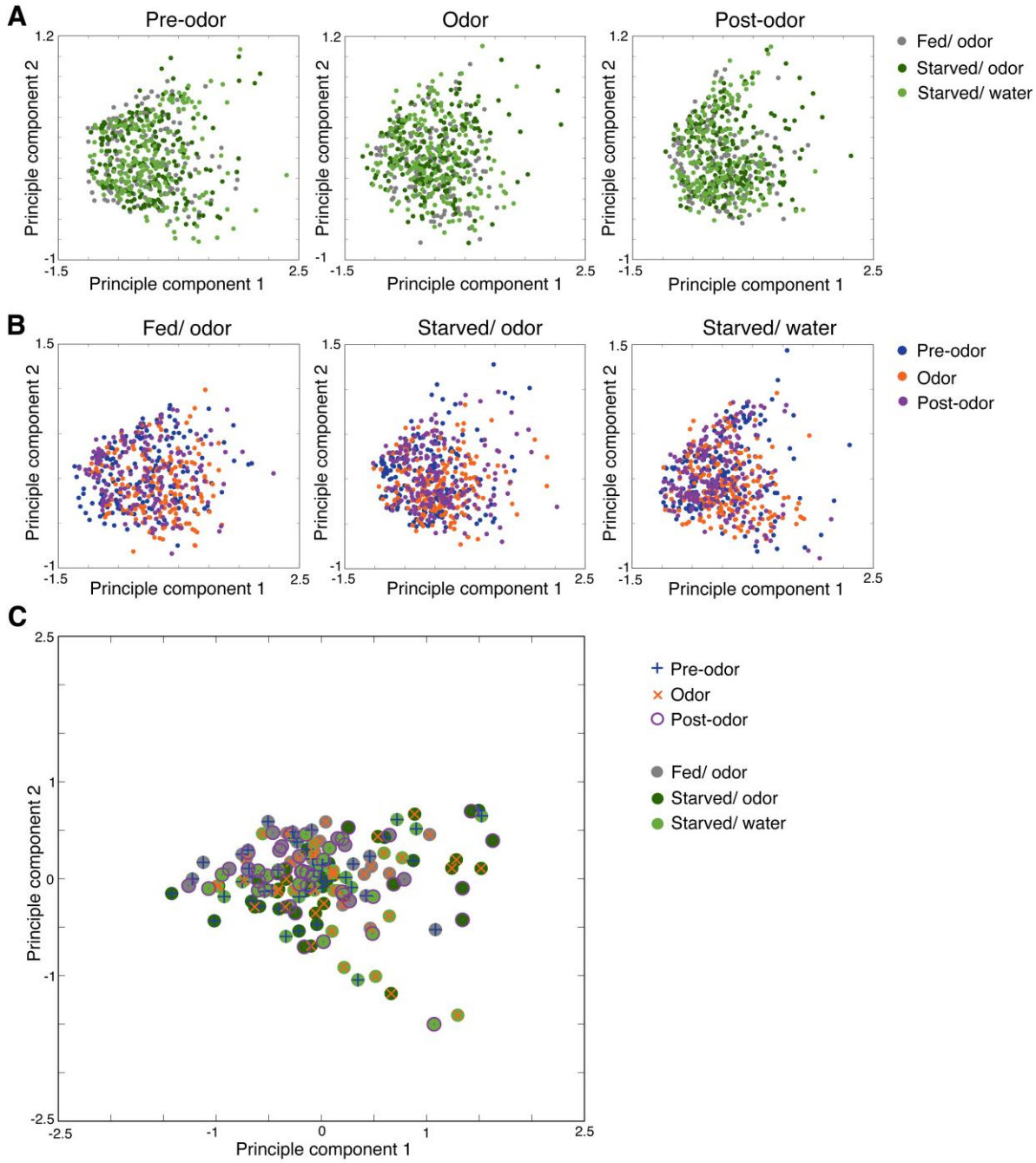

Figure S7. Principle component analysis of fly responses to odor or water (Related to Figure 6)

(A) The walking features of fed flies in response to odor (grey), starved flies in response to odor (dark green), or starved flies in response to water vapor (green) before, during and after stimulation were subjected to principle component analysis (PCA). No group-dependent clustering was observed in any phase.

(B) The walking features of fed flies in response to odor (left panel), starved flies in response to odor (middle panel), or starved flies in response to water vapor (right panel) before (blue dots), during (orange dots) and after (magenta dots) stimulations were subjected to PCA. No phase-dependent clustering was observed in any group.

(C) The walking trajectories of three groups of flies in three phases were subjected to PCA. Features analyzed in (A, B) and (C) were in 5-sec and 1-min time bins, respectively.

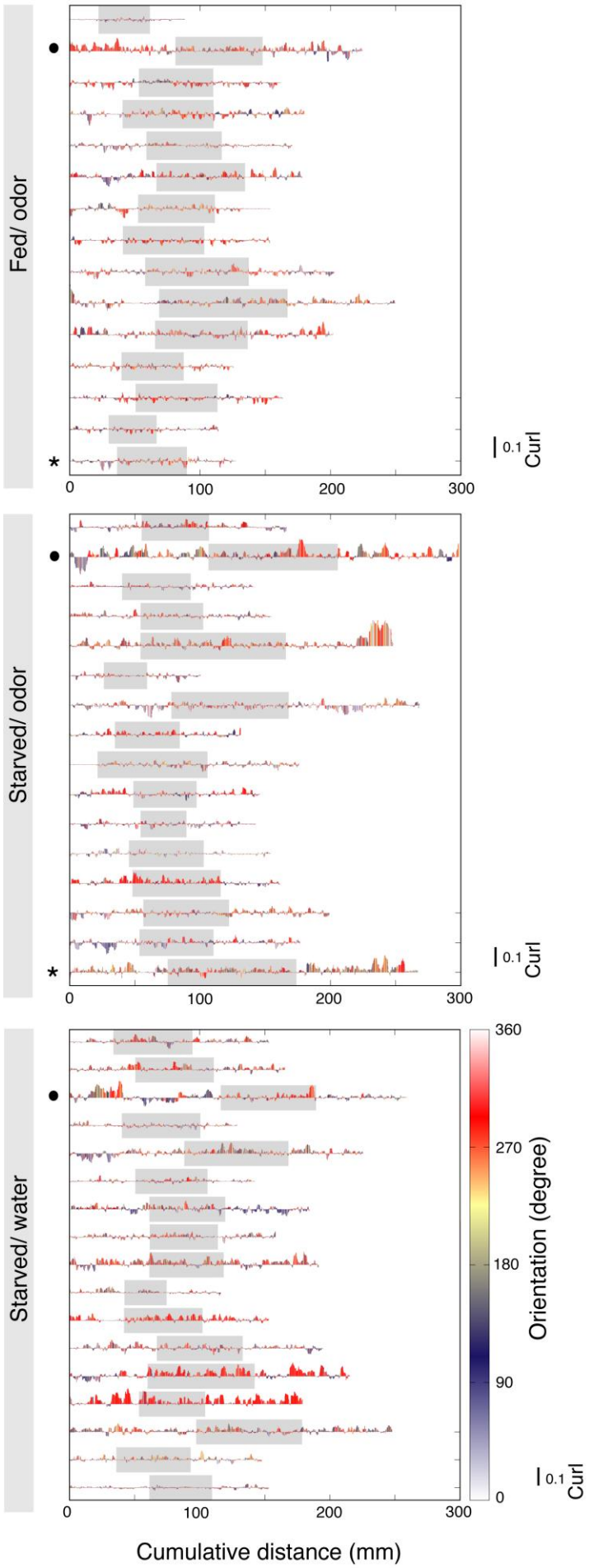
Fed/ odor
Starved/ odor
Starved/ water
0.1
Curl
360
270
180
90
0
Orientation (degree)
0
100
200
300
Cumulative distance (mm)

Figure S8. The walking patterns of individual flies to odor. (Related to Figure 6)

Flies with different internal states (fed or starved) were exposed to odor or water vapor. The dynamics of three walking features (curl, orientation and accumulated distance) were arranged based on individual locomotor activities from high (top) to low (bottom). The odor-phase is in grey shadow. The Y-axis shows the value of curl (positive and negative values indicate two opposite directions). Orientation was color-coded as shown. The trajectories lacking locomotor activity data are indicated with asterisks. The three trajectories shown in Figure 6G are indicated with dots. Scale bar for curl, 0.1.

Supplemental Table

Table S1. Statistical test results for Figures 4B, 5B, 5D, 5F, 5G, 5Hand 6C (Related to Figures 4, 5, and 6)

Figure	Feature	Group	Phase/ time bins	p-value
Figure 4B (unpaired)	Orientation distribution	Fed/ odor	Pre-odor vs Odor	0.01177*
			Pre-odor vs Post-odor	0.2538
			Odor vs Post odor	0.02568*
		Starved/ odor	Pre-odor vs Odor	0.04383*
			Pre-odor vs Post-odor	0.91
			Odor vs Post odor	0.1707
		Starved/ water	Pre-odor vs Odor	0.1136
			Pre-odor vs Post-odor	0.9678
			Odor vs Post odor	0.08598
Figure 5B (paired)	Average of distance	Fed/ odor	11 vs 12	0.1354
			23 vs 24	0.1354
		Starved/ odor	11 vs 12	0.02899*
			23 vs 24	0.09399
		Starved/ water	11 vs 12	0.07968
			23 vs 24	0.1089
Figure 5D (paired)	Straightness	Fed/ odor	11 vs 12	0.1354
			23 vs 24	0.01508*
		Starved/ odor	11 vs 12	0.4037
			23 vs 24	0.5282
		Starved/ water	11 vs 12	0.009338**
			23 vs 24	0.7467
Figure 5F (paired)	Average of curl	Fed/ odor	11 vs 12	0.1876
			23 vs 24	0.8469
		Starved/ odor	11 vs 12	0.782
			23 vs 24	0.3484
		Starved/ water	11 vs 12	0.006653**
			23 vs 24	0.5791
Figure 5G (paired)	Average of |curl|	Fed/ odor	11 vs 12	0.3894

			23 vs 24	0.073
		Starved/ odor	11 vs 12	0.007629**
			23 vs 24	0.9799
		Starved/ water	11 vs 12	0.3529
			23 vs 24	0.003159***
Figure 5H (paired)	Cross correlation between distance and |curl|	Fed/ odor	11 vs 12	0.8469
			23 vs 24	0.7197
		Starved/ odor	11 vs 12	0.7436
			23 vs 24	0.4332
		Starved/ water	11 vs 12	0.4874
			23 vs 24	1
Figure 6C (unpaired)	Accumulated distance	Fed vs Starved		0.5231
	Straightness	Fed vs Starved		0.895
	Frequency of normalized distribution	Fed vs Starved		0.6795
	Accumulated |curl|	Fed vs Starved		0.2994

Mann–Whitney U-test was used. *$p < 0.05$, **$p < 0.01$, ***$p < 0.005$.

Supplemental Videos

Video S1. A tethered fly walking on the treadmill system (Related to Figure 1)

A starved wild-type fly encountered the food odor pentanoic acid (10^{-1} dilution, applied at 17 mL/min). Individual 20-sec videos were extracted from 1-min recordings of pre-odor, odor and post-odor phases, respectively.

Video S2. The video used to test the translation of object motion in 2489 serial frames to a trajectory (Related to Figure 2 and Figure S3)

Transparent Methods

Fly care and genotypes

Flies were raised at 25°C in an incubator with 12 h light-dark cycles. No obvious circadian-dependent differences in walking trajectories were observed (Figure S5). All experiments were conducted in the behavior room, which was constantly controlled at 25°C, 70% humidity and absolute darkness. Genotypes of flies used in this study were Canton S (Bloomington stock center, BL-1), Oregon R (gift from Thomas Clandinin), and wild-caught fly strains DL (Kabra et al., 2012), PR and TB (gifts from Michael Dickinson).

Treadmill systems

The treadmill consisted of an air-supported ball (weight: 0.11 g, diameter: 5.95 mm; 6 mm-PP ball, Holo Pack, Taiwan) suspended on a float mount through the support of four mutually counteracting air streams (designed by K.T.T. and manufactured by the High Precision Machine Shop, Institute of Physics, Academia Sinica). The four-stream air support largely reduced the ball rotation resistance and occasional turbulence, allowing the fruit fly to easily walk on the treadmill. The motion of the air-supported ball was monitored by a high speed CCD camera (GS3-U3-23S6M-C, Point Grey) at 100 frames/sec, which was later used in calculations of the fly walking trajectory. A ring infrared LED (AgileLite system, HOLY STAR) between the ball and camera was used for illumination (Figure 1A, Figure S1). In some experiments, fly walking was simultaneously recorded by a second high speed CCD camera (acA2040-180kmNIR, BASLER) at 30 frames/sec.

The ball was suspended on the float mount through the support of four air streams pumped by an air compressor (JUN-AIR 3-4 Lubricated Quiet Air Compressor). Room air was pumped by the compressor, sequentially stored in a pressure vessel (4 L, Dana-Tank) and an air storage tank (PUMA AST-22), passed through a set of oil mist filters (CKD M4000-15-W), and then released into the air tubing. To generate constant converged air streams, three air regulators were equipped downstream of the pressure vessel, air tank and filter to gradually reduce the pressure (0.12 kg/cm^2 at the end point of 3rd regulator). A five-way joint was used to split the air flow into four streams that fed into the float mount supporting the treadmill ball (Figure S1F).

Odor delivery system

A tubing system was assembled to deliver odor or water vapor to the test fly (Figure S1A, Figure S2A). A continuous stream of compressed air from a gas cylinder (21% O_2 and 79% N_2) was used to drive odor or water vapor delivery. To maintain the air flow at a constant rate, the compressed air was first passed through a mass flow controller (Brooks 5850E) coupled with a power supply (PROTEC PC-510 MFC Readout) with a user interface to display current flow rate and to set a default flow rate (17 mL/min). The air flow with constant flow rate was then infused into a 125-mL glass Erlenmeyer flask with 50 ml liquid solution, such as 10^{-1} pentanoic acid (diluted with distilled water), absolute EtOH, or distilled water. The pressure in the flask drove the odorant or water vapor into the tubing system. A switch system, including four sets of 2-way solenoid valves and two 3-way joints, was inserted at the terminal part of the tubing system to control the odor application in different periods (Figure S2A). The sets of 2-way solenoid valves (SUNWELL SC03-2Z) were used to switch between the on and off of odor/water vapor delivery while maintaining a constant pressure at the terminal part during the switching. Teflon tubes (1/8” OD) were used for the entire tubing system, except for the terminal ends, to keep residual odor low. The terminal ends of the tubing leading in

and out of the odorant/water flask were stainless steel (1/8" OD). The end of tubing system was a 23G needle with a disposable 1.5-cm polyethylene tube. The flow rate used in experiments was 17 mL/min (after 16 mL/min used in Borst and Heisenberg, 1982), and preliminary tests were performed with 10 mL/min (Gaudry et al., 2012) and 22 mL/min (Figure S4B). A photoionization detector (HAL-HVX501, HalTech (for EtOH) or PhoCheck TIGER, Ion Science (for pentanoic acid)) was used to monitor the dynamic concentrations of absolute EtOH (32221, Sigma-Aldrich) and pentanoic acid (240370, Sigma-Aldrich) in the air stream.

Tethering flies

All flies used in this study were 3-8-day-old females, group housed with males and other females before experiments. A stainless steel inset pin (Minutiens ø 0.10 mm, Entomoravia - Austerlitz Insect Pins®) was fixed on the notum of a fly with a drop of UV glue (LIPIT, DENTAMERICA), which was cured by a 20-sec UV exposure (UV gun, LITEX 696, DENTAMERICA). The pin-carrying fly was then tethered on the ball of treadmill and allowed to recover for 1 hr before the experiment. During the 1-hr recovery, the same airflow as administered in the pre-odor phase was constantly applied to the fly. The experiments were conducted in absolute darkness to avoid any visual stimuli. Flies had intact wings and, therefore, wing vibrations occasionally occurred during experiments. We did not observe obvious effects of wing vibration on walking trajectories.

Starving flies

Flies were starved in a 1% agar-based fly vial for 15-25 hr in an incubator with a 12-hr light cycle at 25°C and 70% humidity.

Digitizing fly walking trajectories

The motion of the air-supported ball was entirely driven by the test fruit fly on the top of the ball. Therefore, the ball motion along time accurately reflected the walking trajectory of the fly. In this treadmill system, the motion of the ball was monitored by a high-speed CCD camera (GS3-U3-23S6M-C, Point Grey), equipped with a zoom lens (AF 18-35mm f/3.5-4.5D ED, NIKON) and mounted under the air-supported ball (Figure 1A). The performance of the high speed CCD camera is 1920 × 1200 pixels at 162 frames/sec (GS3-U3-23S6M-C, Point Grey). Frames of 192 × 200 pixels were acquired at 100 Hz (sampling time: 10 msec) with focus on the bottom of ball (radius r = 1.41 mm). A custom-made tracking program was written in C++. The central zone of the acquired ball bottom image in each frame was fitted with the same zone in the previous frame. To minimize the impact of the curvature of the ball surface and allow analysis in a space that approximates a 2-D plane, a small ROI in the ball central zone was extracted from video frames. Accordingly, after calculating the drift between any two consecutive frames, the shifted displacement and the rotation were considered as motion in the X-Y plane and along the rotation axis. The ball motion in the whole recording was then translated as ball motion trajectory through optic flow (https://docs.opencv.org/3.1.0/d7/d8b/tutorial_py_lucas_kanade.html) (Black, 1992).

Climbing test

After each experimental trial, the insect pin was removed from the tethered fly, and a climbing test was performed to assess locomotor activity. In the climbing test, the fly was placed in a 14 mL polystyrene round-bottom tube (PN. 352057, FALCON), with a scale along the height showing mL. Based on the scale,

the test tube was divided to zones: tube bottom to 1 mL was zone 0, 1 mL - 2mL was zone 1, etc. The region from 11 mL – 12 mL was zone 11. The fly was gently shaken to the bottom of vial and allowed to climb toward the top for 15 sec. The locomotor activity score corresponded to the zone where the fly climbed to before the end of the test. The score was zero when the fly stayed at the bottom of the tube; the maximal score was 11 if the fly climbed to or past zone 11.

Distance and displacement

The video of ball motion was subjected to optic flow analysis to calculate the flow vector of each pixel; the vectors were then assembled as the optical flow field between two consecutive frames. Because optical flow can only be used for 2-D areas, the ROI needed to be sufficiently small (radius r = 6 pixels). The horizontal average component and the vertical average component of a given flow field yielded the displacements in the X-dimension and Y-dimension, respectively. The root mean square of the X-dimension and Y-dimension displacements produced the shifting distance in X-Y plane between two frames (Figures 2A, 5A). The displacement in a given time period was the sum of displacements (contains magnitude and direction information) at each sampling time interval (10 msec). Accumulated distance was the sum of magnitude of displacements at each sampling time interval (Figure 5C). Accordingly, distance refers to the length of the route and displacement refers to the shortest length between the start and end points of a route.

Orientation

Orientation is the direction of displacement. The angular coordinate of a polar coordinate system was used to describe orientation, where positive-X coordinate equals 0° and the counterclockwise rotation from this reference was defined as the degree of orientation (θ) (middle panel in Figure 4A). To quantify and better describe the dynamics of orientation distributions in three different odor phases, all orientation events in a phase (60 sec/phase) were aggregated into 6^{o} bins and normalized by the number of total events in that phase (No. of events in one angular bin/No. of total events in a given phase) (right panel in Figure 4A). The orientation angles along time derived for flies of the same experimental group in a given odor phase were compiled as an orientation distribution. The orientation distributions of the same group of flies in any two odor phases were subjected to Mann-Whitney U test to identity possible statistical differences (Figure 4B). On the other hand, the orientation events along time were pooled in both angular bins and time bins (10 sec/bin). Each collection of events in a given angular and time bin was normalized by the number of total events in the corresponding time bin (No. of events in one angular and time bin/No. of total events in the corresponding time bin) (Figure 4C, Figure S4).

Straightness

Straightness was used to quantify the tendency of a fly to walk along a straight path in a given time period. For example, for a given walking trajectory over 5 sec, the straightness equals the magnitude of displacement in 5 sec divided by the accumulated distance in 5 sec (Figure 5C). The closer the straightness was to 1, the straighter the path the fly walked. If straightness was close to 0, the fly walked around within 5 sec but did not move far from the initial position.

Curl

In a small ROI of the ball bottom (radius *r* = 6 pixels), the spherical surface was treated as a 2-D area. Accordingly, the flow field in this Cartesian coordinate system is

$$\vec{F}(x,y,z) = F_x\hat{\imath} + F_y\hat{\jmath} + F_z\hat{k}, \tag{1}$$

where F_x, F_y and F_z are the components of $\vec{F}$ in X-, Y-, and Z-axis, respectively. Because the flow field is in a 2-D plane ($F_z = 0$), curl $\vec{F}$ was used to calculate the magnitude of rotation of the flow field as

$$\nabla \times \vec{F} = \left(\frac{\partial F_y}{\partial x} - \frac{\partial F_x}{\partial y}\right)\hat{k} = \left(\lim_{\Delta x \to 0} \frac{F_y(x_0+\Delta x, y_0) - F_y(x_0,y_0)}{\Delta x} - \lim_{\Delta y \to 0} \frac{F_x(x_0, y_0+\Delta y) - F_x(x_0,y_0)}{\Delta y}\right)\hat{k}. \tag{2}$$

Where $F_x(x_0, y_0)$ and $F_y(x_0, y_0)$ are flow vector in X- and Y-axis at a given pixel (x_0, y_0) in the ROI, respectively. The magnitude of rotation in the flow field, called curl, was calculated as $\sum_{i \text{ in ROI}} \frac{F_y(x_i+1, y_i) - F_y(x_i, y_i)}{1} / \sum_{i \text{ in ROI}} i - \sum_{i \text{ in ROI}} \frac{F_x(x_i, y_i+1) - F_x(x_i, y_i)}{1} / \sum_{i \text{ in ROI}} i$ over all pixels in the ROI.

Rotation center

Since the spherical surface of the ROI was treated as a 2-D area, the rotary axis of estimated rotation centers is along the Z-coordinate and not the radial coordinate. Accordingly, when the estimated rotation center falls in the center of the ROI (X-Y space), the ball exhibits yaw rotation. In other cases where the estimated rotation center falls outside the ROI center, the ball is exhibiting a more roll or pitch rotation. In an extreme case of roll or pitch rotation, the rotation center would fall in infinity. Whenever the rotation center is not infinity, the normal lines of the flow vectors in a given single-rotary-center flow field are expected to cross at a particular rotation center. The position of this rotation center in the X-Y plane (C_x, C_y) is

$$C_x = \frac{\left(y_i - y_j\right) + \left(\frac{u_i}{v_i}x_i - \frac{u_j}{v_j}x_j\right)}{\frac{u_i}{v_i} - \frac{u_j}{v_j}} \tag{3}$$

$$C_y = -\frac{u_i}{v_i}C_x + \left(y_i + \frac{u_i}{v_i}x_i\right), \tag{4}$$

where (x_i, y_i) and $\left(x_j, y_j\right)$ are the position of pixel i and j, respectively. (u_i, v_i) and $\left(u_j, v_j\right)$ are the flow vectors at the positions of pixel i and j, respectively. Since the error may become large when the flow vector is small, all rotation centers $\left(C_x, C_y\right)$ derived from any two pixel positions were further averaged as

$$C_x' = \frac{\sum_{i,j \in \text{ROI}; i \neq j} C_{x,ij} \times W_{ij}}{\sum_{i,j \in \text{ROI}; i \neq j} W_{ij}} \tag{5}$$

$$C_y' = \frac{\sum_{i,j \in \text{ROI}; i \neq j} C_{y,ij} \times W_{ij}}{\sum_{i,j \in \text{ROI}; i \neq j} W_{ij}}, \tag{6}$$

where $C_{x,ij}$ and $C_{y,ij}$ are $\left(C_x, C_y\right)$ derived from the positions of pixel i and j. The weight of each $C_{x,ij}$ and $C_{y,ij}$ is

$$W_{ij} = \sqrt{u_i^2 + v_i^2} + \sqrt{u_j^2 + v_j^2}. \tag{7}$$

Correlation

Cross-correlation (Pearson correlation) was used to estimate the correlation between distance l and |curl| $\mathrm{m} = \left|\nabla \times \vec{F}\right|$ (Figure 5H). The cross-correlation was calculated as

$$\frac{\sum_{t\in\tau}(l_t-\bar{l})(m_t-\bar{m})}{\sqrt{\sum_{t\in\tau}(l_t-\bar{l})^2}\sqrt{\sum_{t\in\tau}(m_t-\bar{m})^2}}, \quad (8)$$

where τ was the time period of every 5 sec. The l_t and m_t indicated the distance and |curl| at time t, respectively. The $\bar{l}$ and $\bar{m}$ were the average of $l_t|_{t\in\tau}$ and $m_t|_{t\in\tau}$, respectively. Accordingly, the cross-correlation between distance and |curl| represented their correlation in all sampling times of a 5-sec time period. In addition, least-squares fitting was used to estimate the correlation between distance and |curl| (Figure 5I, Figure S6). The linear correlations between average and S.D. of distance and |curl| in each 5-sec time period were identified. The linear correlations represented the correlation between two analyzed features in a short time period.

Principal component analysis

The 28 walking variables in each 5-sec time bin for individual flies that were used for principal component analysis (PCA) included: average and standard deviation of rotation centers in X-Y plane, average and standard deviation of distances between rotation centers and the center of ROI, average and standard deviation of curls, weighted average of rotation centers by distance, average and standard deviation of distance, magnitude of directed displacement, accumulated distance, average and standard deviation of orientations, orientation of directed displacement, accumulated orientation, weighted average of orientations by distances, median distance, cross-correlation between distances and curls, weighted average of rotation centers by curls, average and standard deviation of |curl|, cross-correlation between distances and |curl|, accumulated |curl|, and straightness. For PCA, each variable of a fly in a time bin was normalized to the range of the given feature among all the time bins and across all the compared individual flies – for example, (average of distance of a fly in a time bin – minimum of average of distance of flies over time bins) / (maximum of average of distance of flies over time bins – minimum of average of distance of flies over time bins) – such that each value fell between 0 and 1. Normalized values were then subjected to PCA, coded in the C++ language.

Scale-free index

The walking distance in a given time interval T is estimated as

$$|\Delta \mathrm{X}_T| = \sqrt{\big(x(t)-x(t-T)\big)^2+\big(y(t)-y(t-T)\big)^2}, \quad (9)$$

where $\big(x(t),y(t)\big)$ is the position of the fly at time t. To determine whether flies walked on the treadmill in a scale-free manner, the average of walking distance to the power of q was calculated in different time scales as $\langle|\Delta \mathrm{X}_T|^q\rangle$,

$$\langle|\Delta \mathrm{X}_T|^q\rangle \propto T^{a(q)}. \quad (10)$$

After plotting $\langle|\Delta \mathrm{X}_T|^q\rangle$ and T on a log-log plot, the slope ζ is $\zeta = \alpha q$. If $\alpha \approx 0.5$, the fly exhibited a random walk. For α larger than 0.5, the fly walked in a more scale-free manner. In addition to distance, the data of orientation and curl were also applied to test the scale-free nature of the results (Figure 6F).

Supplemental References

Black, M. 1992. Robust incremental optical flow. Ph.D., Yale University.

Borst, A. and Heisenberg, M. (1982). Osmotropotaxis in Drosophila melanogaster. Journal of comparative physiology 147**,** 479-484.

Gaudry, Q., Hong, E. J., Kain, J., De Bivort, B. L. and Wilson, R. I. (2012). Asymmetric neurotransmitter release enables rapid odour lateralization in Drosophila. Nature 493**,** 424.

Kabra, M., Robie, A. A., Rivera-Alba, M., Branson, S. and Branson, K. (2012). JAABA: Interactive machine learning for automatic annotation of animal behavior. Nature Methods 10**,** 64.